

Use of hyperspectral imagery to predict foliar nitrogen, phosphorus and photosynthetic capacity in radiata pine

Michael S. Watt, Henning Buddenbaum, Ellen Mae C. Leonardo, Honey Jane C. Estarija, Horacio E. Bown, Mireia Gomez-Gallego, Robin Hartley, Peter Massam, Liam Wright, Pablo J. Zarco-Tejada

Date: 17th September 2020

Report No: RFP-T004

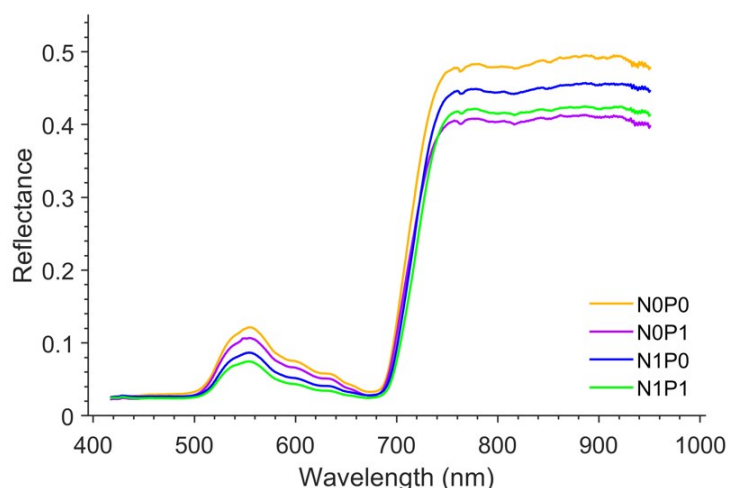
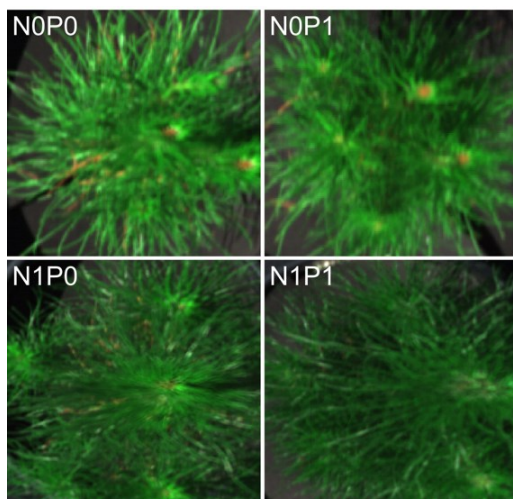


TABLE OF CONTENTS

EXECUTIVE SUMMARY	1
INTRODUCTION	2
METHODS.....	4
2.1. Experimental set up	4
2.2. Hyperspectral imagery collection.....	4
2.2.1 Data capture.....	4
2.2.2. Pre-processing of hyperspectral data	5
2.2.3. Calculation of Solar Induced Chlorophyll Fluorescence	5
2.3. Photosynthetic capacity.....	6
2.4. Determination of foliage N and P and nutrient ratios	6
2.5. Data analysis	6
2.5.1. Relationships between N, P and biochemical limitations to photosynthesis	6
2.5.2. Categorisation of N and P limited plants	7
2.5.3. Prediction of foliage nutrition	7
RESULTS	7
3.1. Foliar nutrition	7
3.2. Hyperspectral data	8
3.3. Testing the independence of N and P limitations.....	8
3.4. Categorisation of N and P limited plants.....	10
3.5. Models of N and P.....	11
3.6. Models of V_{cmax} and J_{max}	13
Discussion	15
Conclusions	17
ACKNOWLEDGEMENTS	18
REFERENCES	19

Disclaimer

This report has been prepared by New Zealand Forest Research Institute Limited (Scion) for Forest Growers Research Ltd (FGR) subject to the terms and conditions of a research fund agreement dated 1 April 2014.

The opinions and information provided in this report have been provided in good faith and on the basis that every endeavour has been made to be accurate and not misleading and to exercise reasonable care, skill and judgement in providing such opinions and information.

Under the terms of the Services Agreement, Scion's liability to FGR in relation to the services provided to produce this report is limited to the value of those services. Neither Scion nor any of its employees, contractors, agents or other persons acting on its behalf or under its control accept any responsibility to any person or organisation in respect of any information or opinion provided in this report in excess of that amount.

EXECUTIVE SUMMARY

The problem

Spatial prediction of photosynthesis requires an understanding of how foliage nitrogen (N) and phosphorus (P) regulate this process and the relationship between these elements and scalable spectral proxies. Hyperspectral imagery has been used to predict important photosynthetic variables such as the maximum rate of carboxylation (V_{cmax}) and electron transport (J_{max}). However, our understanding of how generally applicable these relationships are for plants that are limited by N and P, characterised by respective mass based ratios of $\text{N/P} \leq 10$ and $\text{N/P} > 10$, is still incomplete as most studies assume N and P co-limit photosynthesis.

Hyperspectral imagery and measurements of photosynthesis were obtained from one-year old *Pinus radiata* D. Don, grown under a factorial combination of N and P treatments. Using these data, the objectives of this study were to (i) identify whether trees were co-limited or independently limited by N and P, and then use hyperspectral imagery to (ii) partition N and P limited trees, (iii) build models of N and P from a range of hyperspectral indices and (iv) explore links between key plant traits and both V_{cmax} and J_{max} .

Key results

Compared to the use of all data, which assumes co-limitation, markedly stronger relationships between N and P and photosynthetic capacity were obtained through splitting data at $\text{N/P} = 10$ (independent limitation) for both V_{cmax} ($R^2 = 0.40$ vs. 0.59) and J_{max} ($R^2 = 0.38$ vs. 0.64). A random forest model was used to accurately partition N from P limited trees and the two main variables used within this model were Photochemical Reflectance Index (PRI) and Solar-Induced Chlorophyll Fluorescence (SIF). Using data from the P limiting phase, the most precise models of P were created using PRI ($R^2 = 0.75$) and SIF ($R^2 = 0.52$). Indices that were proxies for chlorophyll were the most precise predictors of N within the N limiting phase but strong positive relationships were also evident between N and both PRI ($R^2 = 0.83$) and SIF ($R^2 = 0.57$). Through their correlations with N and P, there were strong positive relationships between both SIF, PRI and V_{cmax} ($R^2 = 0.78$ and 0.83 , respectively) and J_{max} ($R^2 = 0.80$ and 0.83 , respectively) that were generalisable across both N and P limiting ranges.

Implications of results for the client

These results suggest that quantified SIF and PRI from hyperspectral images may have greater precision and generality for predicting both foliage nutrition and biochemical limitations to photosynthesis than other widely used hyperspectral indices.

Further work

Further research should examine this approach for identifying N and P limitations and developing models that link hyperspectral data to nutrient content and photosynthesis at increased scale. A research project is already underway to extrapolate these findings to the accelerator trials using UAV acquired hyperspectral imagery.

INTRODUCTION

The prediction of foliage nutrient concentration across broad spatial scale has considerable utility for assessing health and productivity of ecosystems (McNeil et al., 2007a; McNeil et al., 2007b; Townsend et al., 2003). Significant growth responses within forest stands have been noted through the application of fertiliser, mainly in the form of nitrogen (N) and phosphorus (P) (Albaugh et al., 2003; Allen et al., 2005; Liechty and Fristoe, 2013). However, determining the optimal application of fertiliser is often very difficult as nutritional deficiencies vary widely across the landscape (Campion, 2008; Fox et al., 2007).

Foliage nutrition is also a key determinant of rates of carbon assimilation. Many studies have investigated the use of N and P to account for variation in photosynthetic capacity (Walker et al., 2014) and the importance of these elements on the photosynthesis process is well documented. Nitrogen is a major component of Rubisco (Niinemets and Tenhunen, 1997) and P has an impact on many important aspects of photosynthesis including membrane solubility, ATP, and NADPH production (Marschner, 1995; Taiz et al., 2015). Given these strong links it is important to understand how N and P regulate photosynthesis when developing models of these elements that will be subsequently used to predict photosynthesis.

Hyperspectral imagery has been successfully used to predict foliar concentrations of N for a wide range of broadleaf and coniferous species at both the leaf level and canopy level (for an overview see Hill et al., 2019; Watt et al., 2019). Nitrogen shows marked absorption features in both the visible near infrared (VNIR) and short-wave infrared (SWIR) ranges (Curran, 1989; Kokaly, 2001; Kokaly et al., 2009) and models are able to capitalise on these features to predict N (Watt et al., 2019). At the leaf level the precision of models of N has been found to range widely (R^2 range of 0.37 to 0.99) but generally N has been predicted with moderate to high levels of precision, with mean R^2 of 0.77, recorded across a wide range of species (Asner and Martin, 2008; Asner et al., 2011; Curran et al., 2001; Dechant et al., 2017; Gillon et al., 1999; Luther and Carroll, 1999; Masaitis et al., 2014; Petisco et al., 2005; Schlerf et al., 2010; Serbin et al., 2014; Stein et al., 2014; Tsay et al., 1982; Wang et al., 2018; Wang et al., 2015; Yoder and Pettigrew-Crosby, 1995). Despite the difficulties in scaling to the canopy, moderate to strong predictions of N have also been made at this level with values of R^2 ranging from 0.48 to 0.98 (Coops et al., 2003; Huang et al., 2004; Knyazikhin et al., 2013; Martin et al., 2008; Martin et al., 2018a; Martin et al., 2018b; Ollinger et al., 2008; Singh et al., 2015; Smith et al., 2003).

Although many studies have developed models of P, the lack of spectral absorption features associated with P is likely to limit their generality as these relationships are indirect. Leaf level hyperspectral data have generally been found to predict P empirically with moderate to high precision (mean R^2 of 0.74) using proxies correlated with P, with R^2 varying from 0.32 to 0.95 (Asner and Martin, 2008; Asner et al., 2011; Curran et al., 2001; Gillon et al., 1999; Masaitis et al., 2014; Petisco et al., 2005; Stein et al., 2014). However, as P does not directly absorb energy in the shortwave spectrum, these predictions of P are actually due to the correlations with N found under most conditions (Asner and Martin, 2008; Gillon et al., 1999; Porder et al., 2005). As a consequence, these models may not be as robust when applied to conditions where ratios of N/P deviate from typical ranges. Development of models of P using datasets with little correlation between N and P are likely to reveal the true precision between hyperspectral-based traits and P, likely resulting in predictions that have greater generality.

Although little research considers whether N and P co-limit or independently limit photosynthesis, this is a key assumption that is likely to affect model precision, generality and applicability. Datasets used generally assume that photosynthesis is co-limited by N and P as both elements are predicted across their complete range. Although it has not been widely investigated, a number of studies suggest that N and P independently limit growth and photosynthesis in many species (Bown et al., 2007; Domingues et al., 2010; Ingestad, 1971, 1979; Ingestad and Lund, 1986). The premise underlying this research is that a mass based N/P ratio of 10 is optimal with values of $N/P \leq 10$ leading to N limitations and $N/P > 10$ resulting in P limitations (Aerts and Chapin, 2000; Marschner,

1995; Reich and Schoettle, 1988). Previous research supports this suggestion through showing that N and P independently influence the key biochemical limitations to photosynthesis that include the maximum rate of carboxylation (V_{cmax}) and electron transport (J_{max}) (Domingues et al. 2010) and that a stoichiometric ratio of 10 can be used to partition N from P limitations for these variables (Bown et al. 2007). If photosynthesis is independently regulated by N and P it follows that V_{cmax} and J_{max} will exhibit positive relationships with both elements within their respective limiting ranges and these relationships will be weaker when they are constructed using the entire dataset under the assumption of co-limitation.

The assumption of independent limitations has important implications for the development of foliage nutrition models. In order to identify the type of required nutrient additions it would be useful to be able to partition N from P limitations at scales ranging from the tree to the forest level. Following this partitioning, the use of N and P models developed using data from their respective limiting ranges could be applied to estimate the severity of any deficiency and impact on photosynthesis within these two ranges. This approach may provide a means of improving spatial accuracy when characterising the type and extent of nutrient deficiencies. Understanding the nature of relationships, within each limiting range, is also likely to provide considerable insight into the mechanistic link between plant functional traits quantified from hyperspectral imagery and foliage nutrition and, as a consequence, growth and photosynthesis. Despite this, we are unaware of any research that has used this approach for developing models of N and P for tree species.

Traditional methods used to track changes in plant nutrition from remote sensing have most often targeted chlorophyll content ($C_{\text{a+b}}$) as chlorophyll and other pigments such as carotenoids, xanthophyll and anthocyanins are important indicator of plant photosynthetic status (Baret et al., 2007; Evans, 1989; Yoder and Pettigrew-Crosby, 1995). Nitrogen is a major component of chlorophyll, and nitrogen and chlorophyll deficiencies are directly related to reductions in photosynthesis (Evans, 1989). It therefore follows that $C_{\text{a+b}}$ has been the focus of remote sensing research as a proxy for nitrogen within agriculture and forestry (Baret *et al.*, 2007; Yoder and Pettigrew-Crosby, 1995).

Remote sensing research carried out in the 1980s identified the red-edge and green spectral regions as potential targets for estimating $C_{\text{a+b}}$ that were linked to nitrogen content (Carter, 1994; Gitelson and Merzlyak, 1996; Rock et al., 1988). Further research developed specific narrow-band hyperspectral indices (Haboudane et al., 2002) including the red-edge Chlorophyll Index (Zarco-Tejada et al., 2001). Combined indices were also developed such as the Transformed Chlorophyll Absorption in Reflectance Index, TCARI (Haboudane *et al.*, 2002) normalized by the Optimized Soil-Adjusted Vegetation Index, OSAVI (Rondeaux et al., 1996) to form the TCARI/OSAVI proxy for chlorophyll and nitrogen.

In addition to $C_{\text{a+b}}$, recent research has identified other pigments, such as xanthophylls, that are more dynamically related to rapid changes in photosynthesis and are potentially more useful for tracking nutritional impacts on photosynthesis. The changes observed in the green spectral region through the Photochemical Reflectance Index (PRI) (Gamon et al., 1992) have been demonstrated to be linked to the xanthophyll cycle, and this index has been successfully used to predict photosynthetic rate (Drolet et al., 2008; Fuentes et al., 2006; Gamon et al., 1997; Guo and Trotter, 2004; Hilker et al., 2008; Middleton et al., 2009; Nichol et al., 2000; Penuelas et al., 1995b; Stylinski et al., 2000) and the photosynthetic response of plants to a range of stresses (Buddenbaum et al., 2015; Dobrowski et al., 2005; Hernández-Clemente et al., 2011; Scholten et al., 2019; Suarez et al., 2008).

During the last 50 years (see review by Mohammed et al., 2019) considerable research has demonstrated the utility and feasibility of Solar-Induced Chlorophyll Fluorescence (SIF) in predicting photosynthetic activity at both the leaf and the canopy scales from a range of remote sensing platforms (Cendrero-Mateo et al., 2015; Zarco-Tejada et al., 2013; Zarco-Tejada et al., 2016). Given the strong relationship between chlorophyll pigments, the xanthophyll dynamics (PRI) and photosynthesis (through SIF) it also follows that these indicators might be significantly related to N and P as these two elements are key determinants of photosynthesis rate.

Pinus radiata D. Don (radiata pine) is the most widely planted plantation species within the southern hemisphere (Lewis and Ferguson, 1993). Over 4.1 M ha of this species has been established in New Zealand, Chile and Australia, where the species comprises, respectively, 90% (NZFOA, 2018), 62% (Salas et al., 2016) and 39% (Downham and Gavran, 2019) of the total plantation area. *Pinus radiata* frequently suffers from nutrient limitations, particularly during mid-rotation when nutrient demand often exceeds supply. The key elements that limit productivity of *P. radiata* are N and P (Watt et al., 2005). A shortage of these elements can result in significant reductions in growth (Raison and Myers, 1992; Sheriff et al., 1986) and also limits the key processes that control the rate of photosynthesis (Bown et al., 2009).

In this study, measurements of hyperspectral imagery, photosynthesis and foliage nutrition were taken from an experiment that included a factorial combination of N and P treatments applied to *P. radiata*. Using these data, the initial objective of this research was to (i) identify whether trees were co-limited or independently limited by N and P, and then use hyperspectral imagery to (ii) partition N and P limited trees, (iii) build models of N and P from a range of hyperspectral indices and (iv) explore links between key plant traits and both V_{cmax} and J_{max} .

METHODS

2.1. Experimental set up

The experiment was undertaken within the Scion nursery, located in Rotorua, New Zealand. A total of 120 *P. radiata* seedlings were transplanted into 15 L pots during October 2018. The medium into which the plants were transplanted consisted of a mixture of perlite and vermiculite which are silica-based products without any nutritional content. Plants were grown in a thermostatically controlled greenhouse where temperature in spring fluctuated between 10 and 24°C during the day and between 10 and 16°C during the night. These plants were watered weekly over the duration of the trial so that root-zone water content did not limit growth. This study reports on detailed measurements taken from 60 trees during October 2019, within this trial, that included twelve trees from each of the five treatments.

The five fertiliser treatments consisted of a factorial combination of N and P that were applied as 500 ml of nutrient solution per plant every fortnight starting on the 20th February 2019. These five treatments included application of water only (Control), low N–low P (N0P0), low N–high P (N0P1), high N–low P (N1P0) and high N–high P (N1P1). Nutrient solutions consisted of two levels of nitrogen (N0 = 1.43 and N1 = 7.14 mol m⁻³) and phosphorus (P0 = 0.084 and P1 = 0.420 mol m⁻³). Following Ingestad (1979), N was provided at concentrations of 100 ppm (7.14 mM) and P at 13 ppm (0.420 mM) as the high-N and high-P supply regimes. The low-N (1.43 mM) and low-P (0.084 mM) supply regimes were chosen as one-fifth of the high-N and high-P concentrations, respectively. Nitrogen was supplied as NH₄NO₃ and phosphorus as KH₂PO₄ and nutrients other than N and P were provided in optimum proportions in relation to N, as defined by Ingestad (Ingestad, 1971, 1979).

2.2. Hyperspectral imagery collection

2.2.1 Data capture

A hyperspectral camera (FX10, Specim, Spectral Imaging Ltd, Oulu, Finland) was used to acquire hyperspectral imagery outside during clear sky conditions from 10:30 am to 1:30 pm on the 4th October 2019. This push-broom camera captures 448 bands with wavelengths ranging from 400 to 1000 nm with a spectral full width at half maximum (FWHM) of 5.5 nm and a spectral sampling interval of 2.7 nm. The camera is designed for industrial applications and as such has a high maximum frame rate of 9900 frames per second with one band, and 330 frames per second using the full spectral range, as well as a high Signal-to-Noise Ratio (SNR) of 600:1. Within the field of view of 38° the spatial sampling comprises 1024 pixels. We used the Lumo Recorder software interface to manage the image acquisition.

The camera was mounted 2 m above ground on a cross beam that was supported by two posts and a conveyor belt was used to move the plants through the field of view. The speed of the conveyor belt was adapted to fit the frame rate of the camera, which in turn was dependent on the exposure time, which had to be adjusted to the current illumination conditions. During the measurements, the conveyor belt speed and frame rate were kept constant and the exposure time was adjusted to avoid over or undersaturation. A diffuse white reference standard (Spectralon, North Hutton, NH, USA) was placed so that it was visible in every frame allowing calibration of the imagery as a function of the changing illumination conditions. Images were recorded in nadir view. Since the trees were placed in the centre of the field of view, most pixels were recorded with view zenith angles <math><10^\circ</math>. Solar zenith angles ranged from 32.5° to 38°.

2.2.2. Pre-processing of hyperspectral data

All pre-processing of the hyperspectral data was carried out using Matlab (The MathWorks, Inc., Natick, Massachusetts, United States) following the methods described in Buddenbaum et al. (2019). Measured digital numbers were transformed to reflectance factors by dividing each pixel's value by the respective value of the white reference bar in the same image line, which were then multiplied by the reflectance of the reference bar. Directional effects in the resulting spectra were corrected according to the methods described Buddenbaum et al. (2019). Pixels with NDVI ≥ 0.5 and near-infrared reflectance (780 nm) ≥ 0.2 were selected as vegetation pixels. Pixels with absolute first difference values ≥ 0.1 were masked out. The mean of all pixels for each tree was calculated to represent the canopy reflectance of the whole plant.

Following these steps, the tree level spectra were smoothed using the Savitzky-Golay filter (Mouazen et al., 2010; Vasques et al., 2008). Smoothing used a third order polynomial which was applied across a moving window of 27 spectral bands. Reflectance and the 1st derivative of reflectance were extracted from these smoothed spectra. As there was considerable noise at the upper end of the smoothed spectral data, the bands above 951 nm were excluded from further analyses. Following these exclusions, 408 bands in the 400 – 951 nm spectral range were available for analyses. The reflectance spectra were interpolated to a 1 nm resolution within Matlab to allow spectral indices to be determined using the wavelengths listed in the literature. Using these interpolated spectra the 83 indices listed in Appendix 1 were derived. These narrow-band indices were selected as previous studies have shown these to be related to foliage nutrition, pigment content, leaf and canopy structure, and photosynthesis (see Appendix 1 for references).

2.2.3. Calculation of Solar Induced Chlorophyll Fluorescence

Solar-Induced Chlorophyll Fluorescence (SIF) was quantified using the 760 nm O₂-A region using the *in-filling* method based on the Fraunhofer Line Depth principle (FLD) (Plascyk, 1975). As previously described (Zarco-Tejada et al., 2013; Zarco-Tejada et al., 2016) SIF was calculated from a total of three spectral bands (FLD3) as follows,

$$SIF = \frac{E_{out} L_{in} - E_{in} L_{out}}{E_{out} E_{in}} \quad (1)$$

where radiance, L , corresponds to L_{in} (L_{761}), L_{out} (average of L_{747} and L_{780} bands), and the irradiance, E , to E_{in} (E_{761}), and E_{out} (average of E_{747} and E_{780} bands). Values of SIF were rescaled through addition of an offset value to ensure that calculations of SIF from Equation 1 were not negative.

The determination of SIF from hyperspectral instruments has been demonstrated by several studies that show that fluorescence can be quantified using imaging sensors for stress detection (Calderón et al., 2013; Damm et al., 2015; Zarco-Tejada et al., 2012). Previous modelling work has assessed the requirements of spectral bandwidth, spectral interval and noise levels for determination of SIF (Damm et al., 2011). This research has demonstrated that FLD-based methods are feasible for retrieving SIF using wider spectral bands (i.e. around 5 nm FWHM) as long as high-spectral sampling intervals are used with signal-to-noise ratios that have a minimum

of 300:1.

2.3. Photosynthetic capacity

Measurements of photosynthetic capacity were made on a sub-sample of 30 plants, that included six plants per treatment. These measurements were made using a coupled chlorophyll fluorescence and gas-exchange system (Imaging-PAM M-Series and GFS-3000, Walz, Effeltrich, Germany) from the 7th to 16th of October 2019 following measurements of hyperspectral data. For each of the 30 plants, the response of assimilation to intercellular CO₂ concentration (A_{C_i} response) was measured on two to three fully expanded young fascicles that were selected from the upper third of the canopy. These needles were arranged inside the 6 cm² cuvette without overlap and the area for these needles was determined by differentiating thresholded pixels using the Imaging-Win software of the coupled system. During the course of the measurements, conditions in the cuvette were maintained at 20 °C, with a relative humidity of 60% and an irradiance of 1,000 $\mu\text{mol photons m}^{-2} \text{s}^{-1}$. The external CO₂ concentration (C_a) supplied to the plants included the following series: 400, 300, 200, 100, 75, 50, 400, 600, 800, 1000, 1200, 1500, 2000 $\mu\text{mol mol}^{-1}$. Measurements were recorded after values of A , C_i and g_s were stable. A_{C_i} curves were analysed using Farquhar-type equations (Long and Bernacchi, 2003). A generalised nonlinear least squares regression (*gnls* function, nlme package in R) was used to estimate V_{cmax} and J_{max} .

2.4. Determination of foliage N and P and nutrient ratios

Analysis of foliage N and P was undertaken on approximately 10 fully extended fascicles, that were selected from the upper third of the crown of each plant. These fascicles were dried at 70 °C for at least 48 hours to constant dry mass and transported to the Manaaki Whenua Landcare Research laboratory (Palmerston North, New Zealand) for analysis of N and P. Foliage samples were finely ground, acid digested by the Kjeldahl method, and the N and P concentrations were determined colorimetrically (Blakemore et al., 1987).

Specific leaf area, (SLA) was determined from 20 fully expanded fascicles per plant and expressed on a hemi-surface leaf area basis. Following Bown et al. (2009), leaf area was determined from $[nld(1 + \pi/n)]/2$, where d is fascicle diameter, l is fascicle length and n is the number of needles per fascicle. SLA was expressed in $\mu\text{g cm}^{-2}$ as the quotient of dry weight and leaf area. Measurements of SLA were used to convert foliage nutrient concentrations to a hemi-surface area basis.

2.5. Data analysis

All analyses were undertaken at the plant level using a combination of Matlab (The MathWorks, Inc., Natick, Massachusetts, United States) and R (R Development Core Team, 2011). Matlab was used to plot the hyperspectral spectra while the analyses were undertaken using R. The precision of developed models was compared using the coefficient of determination (R^2) and root mean square error (RMSE). Analyses that categorised N and P limited plants used the variance inflation factor (VIF) to reduce the indices to a set that were not highly correlated using a threshold of five (Akinwande et al., 2015).

2.5.1. Relationships between N, P and biochemical limitations to photosynthesis

The strength of relationships between foliage nutrition (N, P) and the biochemical limitations to photosynthesis (V_{cmax} , J_{max}) was examined to determine if these elements co-limit or independently limit photosynthesis. Using all the data, linear models were developed to determine precision assuming co-limitation of photosynthesis by N and P. Nutrient ratios were used to separate the dataset into plants that were either N or P limited to test the hypothesis that photosynthesis was independently limited by these elements. Following previous literature (Aerts and Chapin, 2000; Knecht and Göransson, 2004; Marschner, 1995; Reich and Schoettle, 1988) trees with an N/P ratio (expressed on a mass basis) of ≤ 10 were categorised as N deficient, while those with $N/P > 10$ were categorised as P deficient. We also split the data at $N/P = 5$ and $N/P = 15$ to examine how partitioning at these two ratios either side of $N/P = 10$ impacted the strength of relationships.

2.5.2. Categorisation of N and P limited plants

Random forest (Liaw and Wiener, 2002) was used to partition trees into N or P limited classes, segregated at $N/P = 10$, using the hyperspectral indices and SIF. Prior to this analysis these 84 variables were reduced to a subset of six using a procedure that sequentially eliminated correlated variables with a VIF that exceeded five (Akinwande et al., 2015). The random forest model was fitted to this reduced set of predictors using a five-fold cross validation. The model fit was assessed using the area under the receiver operating characteristic curve (AUC). The AUC ranges from 0 – 1 and values in excess of 0.9 considered to represent an excellent classification accuracy. The sensitivity of the model to different hyperspectral variables was determined through examination of variable importance.

2.5.3. Prediction of foliage nutrition

Following Kattenborn et al. (2019), all modelling used nutrient concentrations expressed on an area basis. Analyses examined the correlation of foliage nutrition (N, P) and biochemical limitations to photosynthesis (V_{cmax} , J_{max}) with predictor variables derived from the hyperspectral data that included SIF and the 83 derived Indices (Appendix 1). Predictions of N and P were made using respectively, N and P limited plants and the precision of these models were compared to predictions made using the entire dataset for both elements. Relationships were developed using a range of functions that included linear, polynomial and exponential forms, to ensure that predictions were relatively unbiased. The strongest two predictor variables from these analyses were identified and plotted against foliage nutrition (N, P) and biochemical limitations to photosynthesis (V_{cmax} , J_{max}).

RESULTS

3.1. Foliar nutrition

The applied treatments resulted in a wide range in N and P (Fig. 1). Values of N ranged from 0.41 – 2.12 % when expressed on a mass basis and $11.1 - 49.0 \mu\text{g cm}^{-2}$ on an area basis while P varied from respectively 0.052 – 0.330 % and $1.33 - 7.66 \mu\text{g cm}^{-2}$. The relationship between N and P was insignificant when data was expressed on a mass ($R^2 = 0.0073$; $P = 0.52$) or area basis ($R^2 = 0.0006$; $P = 0.85$). Of the 60 plants, 43 were categorised as N limited while 17 were P limited and the separation of these groups is shown by a dotted line in Figure 1.

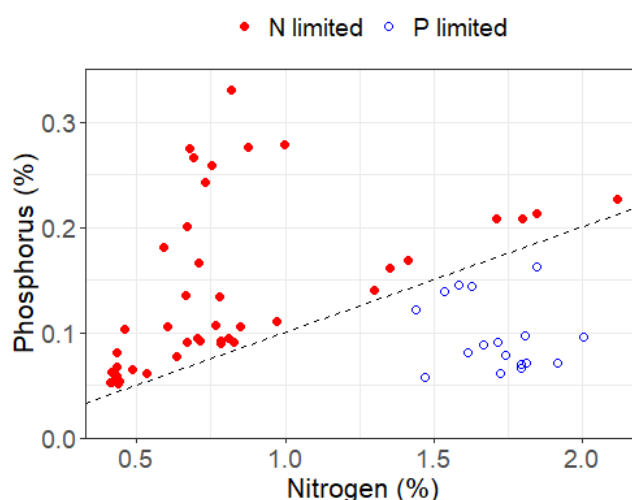


Figure 1. Plot of foliage nitrogen against phosphorus concentration by type of limitation. The dashed line represents a N/P ratio of 10. Values of foliage N and P content above the line are N limited (filled red circles) while those below the line are P limited (open blue circles).

3.2. Hyperspectral data

Trees that were limited by N had higher reflectance than P limited trees within the visible and red edge range from 482 nm – 732 nm (Fig. 2). Differences in the first derivative between the two groups occurred across a wider range than reflectance (Fig. 2). As expected, the first derivative for plants that were N limited was higher from 427 – 554 nm, lower from 562 – 675 nm and exhibited a leftwards shift in the red edge from 678 – 764 nm (Fig. 2).

3.3. Testing the independence of N and P limitations

Relationships between N and both V_{cmax} and J_{max} were positive and significant for all data (Fig. 3a) and for data partitioned at N/P ratios of 5, 10 and 15 (Figs. 3b, c, d). Compared to the relationship using all data, the precision of these relationships markedly increased when data was partitioned into values with N/P ratio ≤ 5 (Table 1). Precision gains were more modest using data with N/P ratio ≤ 10 . Although R^2 was similar to values using all data (Fig. 3c), the more sensitive indicator, RMSE was lower using data with N/P ratio ≤ 10 for both V_{cmax} (3.7 vs. 4.0 $\mu\text{mol m}^{-2} \text{s}^{-1}$) and J_{max} (10.3 vs. 12.0 $\mu\text{mol m}^{-2} \text{s}^{-1}$). There were small increases in RMSE for these relationships as N/P ratio increased from 10 to 15 (Table 1). For data that was limited by P with N/P > 10 , the relationship between N and both V_{cmax} and J_{max} was non-significant, with R^2 of respectively, 0.01 and 0.02 (data not shown).

Using all data, relationships between P and both V_{cmax} and J_{max} were insignificant and weak with R^2 ranging from 0.04 – 0.05 (Fig. 3e). Using data from the P limiting range partitioned at N/P > 5 the precision of these two relationships markedly increased (Fig. 3f). There were further increases in precision when data was restricted to the P limiting range at N/P > 10 (Fig. 3g, Table 1) and values of R^2 for V_{cmax} and J_{max} using this range were, respectively, 0.50 and 0.58 (Table 1). Compared to N/P = 10 there were reductions in precision as N/P further increased to 15 (Table 1). For data that was limited by N at an N/P ratio of 10 (i.e. N/P ≤ 10), the relationship between P and both V_{cmax} and J_{max} was non-significant, with R^2 values of respectively, 0.33 and 0.31 (data not shown).

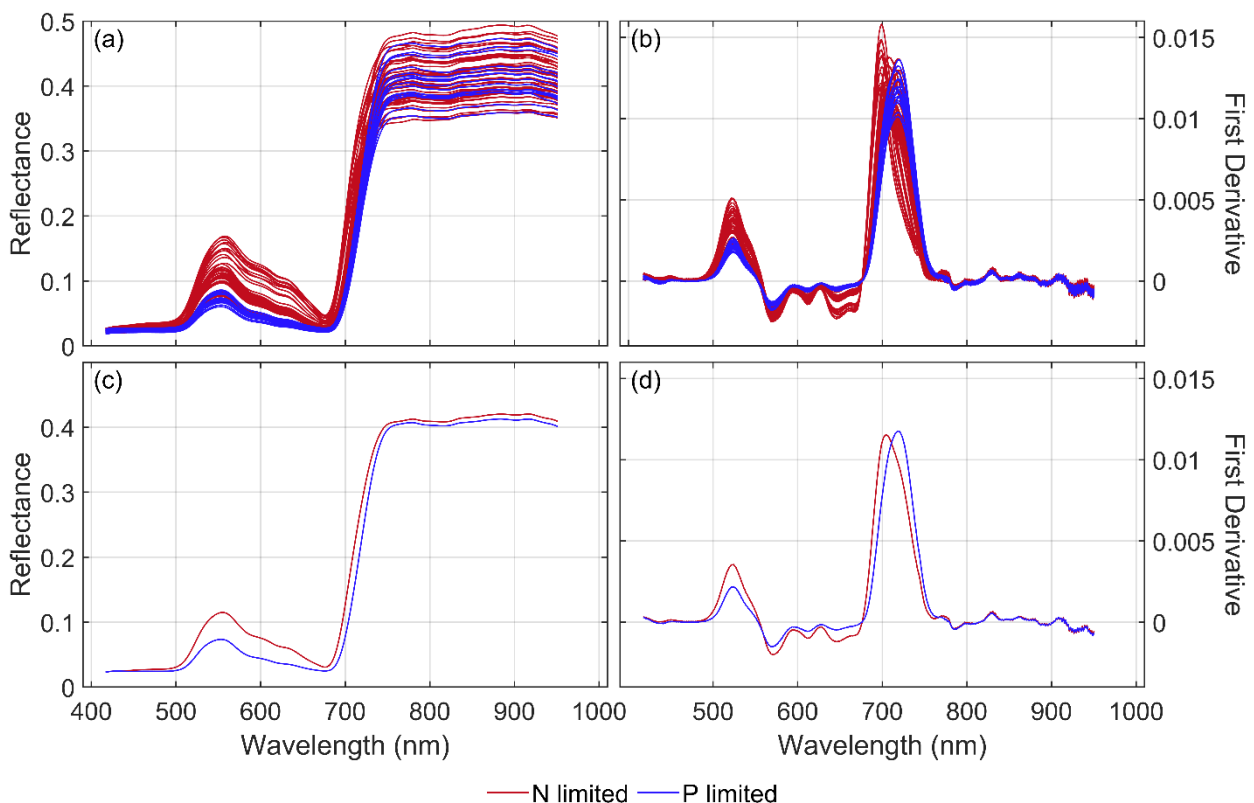


Figure 2. Variation in (a, c) reflectance and (b, d) the 1st derivative of reflectance against wavelength for N (red) and P (blue) limited plants at the (a, b) tree level and (c, d) treatment level.

The mean precision of models using N and P to describe V_{cmax} increased from an average R^2 of 0.40 using all data to values of 0.51 and 0.59, respectively, using data partitioned at N/P = 5 and 10 and then declined to an R^2 of 0.41 at N/P = 15 (Table 1). Similarly, there were marked gains in precision of models using N and P to predict J_{max} with mean R^2 increasing from 0.38 for relationships using all data to values of 0.59 and 0.64, respectively, using data partitioned at N/P = 5 and 10, which declined to an R^2 of 0.58 at N/P = 15 (Table 1). These results suggest that biochemical limitations to photosynthesis are independently limited by N and P and confirm that a N/P ratio of 10 is most appropriate for partitioning data into N and P limiting ranges.

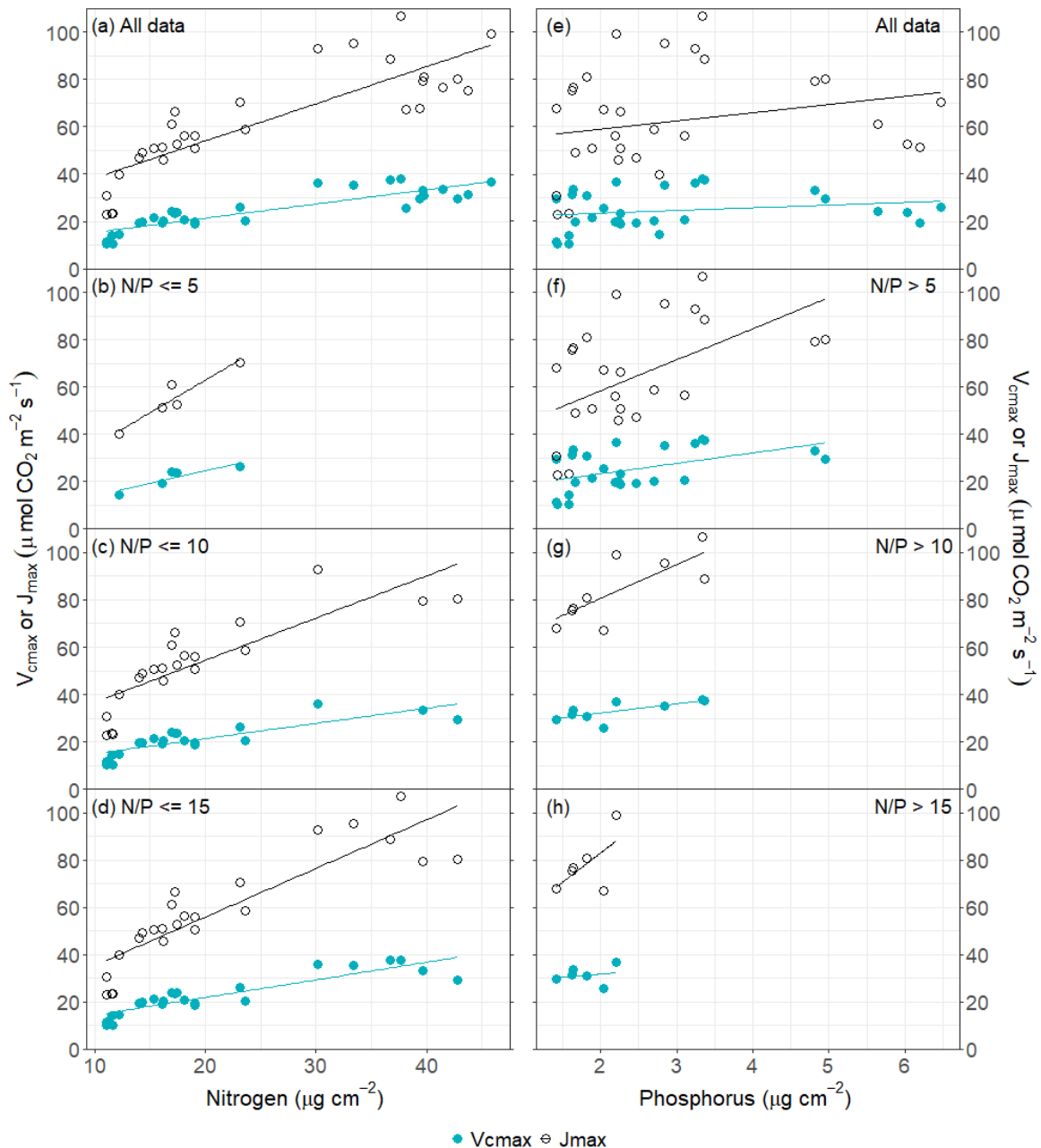


Figure 3. Relationship between nitrogen (left panels), phosphorus (right panels) and both V_{cmax} (filled teal circles) and J_{max} (open black circles) by N/P ratio, with values shown for (a, e) all data and data partitioned at (b, f) N/P = 5, (c, g) N/P = 10 and (d, h) N/P = 15. Linear relationships are fitted to both V_{cmax} (teal lines) and J_{max} (black lines) and the precision of these relationships are given in Table 1.

Table 1. Statistics of models using N and P to predict V_{cmax} and J_{max} using all data, and data partitioned at N/P = 5, 10 and 15. Shown for each model are the R^2 and root mean square error (RMSE). Also shown are the average R^2 and RMSE values across both N and P limiting ranges for the three datasets.

Dependant variable	Ratio	Model with N		Model with P		Average for N, P	
		R^2	RMSE	R^2	RMSE	R^2	RMSE
V_{cmax}	All data	0.76	4.0	0.04	8.0	0.40	6.0
	N/P = 5	0.79	1.9	0.23	7.6	0.51	4.8
	N/P = 10	0.68	3.7	0.50	2.7	0.59	3.2
	N/P = 15	0.78	3.8	0.04	3.4	0.41	3.6
J_{max}	All data	0.71	12.0	0.05	21.6	0.38	16.8
	N/P = 5	0.89	3.4	0.28	20.1	0.59	11.8
	N/P = 10	0.69	10.3	0.58	8.6	0.64	9.5
	N/P = 15	0.78	10.6	0.38	8.5	0.58	9.6

3.4 Categorisation of N and P limited plants

The random forest model used to partition N from P limited plants was very accurate and had an AUC of 0.96. A total of five variables, were used in the model (Fig. 4a) and the two most important variables in this model were PRI and SIF. A plot of the two strongest variables, highlighted the utility of these variables in separating N from P limitations (Fig. 4b).

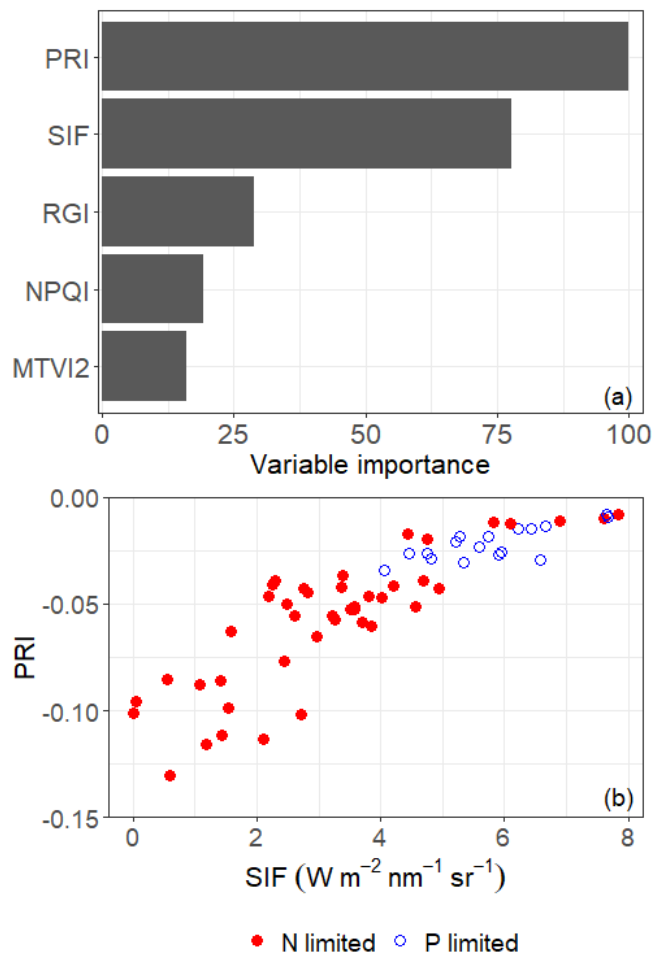


Figure 4. (a) Importance of variables used to partition N from P limitations and (b) relationship between the two most important variables, Solar-Induced Chlorophyll Fluorescence (SIF) and Photochemical Reflectance Index (PRI), by the type of limitation.

3.5. Models of N and P

Indices that were most strongly related to N, using observations from the N limited dataset, included the Carter Index 1 (R_{695}/R_{420}) and Lichtenthaler Index 2 (R_{440}/R_{690}), which had respective R^2 of 0.89 and 0.88 (Table 2, Fig. 5). However, these two indices were not significantly related to N when predictions were constrained to P limited plants (Table 2) and Figure 5 shows that these data added scatter into relationships using N limited data at high values of N. Predictions of N with these indices using all data had a similar R^2 to predictions using only N limited data (Table 2). However, the RMSE of these predictions was markedly lower using N limited data than all data for both Lichtenthaler Index (3.21 vs 4.01 $\mu\text{g cm}^{-2}$) and Carter Index (3.09 vs. 3.86 $\mu\text{g cm}^{-2}$) reflecting the greater scatter of P limited data at higher values of N (Fig. 5). Using N limited data, the relationship between the Carter Index and N was non-linear and negative and best fitted by an exponential decay function (Fig. 5a) while the relationship between Lichtenthaler Index and N was positive and best fitted with a second order polynomial (Fig. 5b).

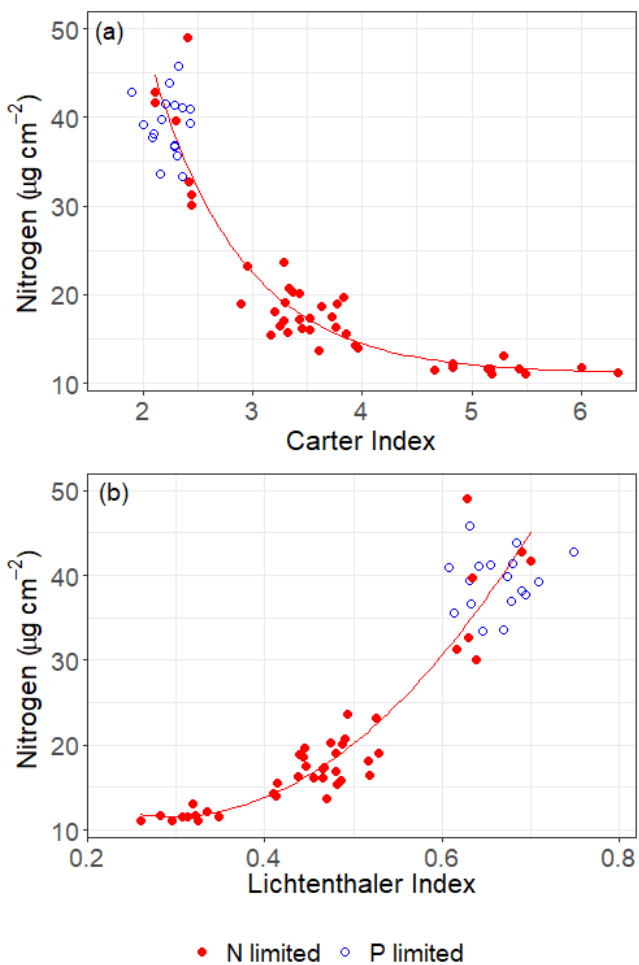


Figure 5. Relationships between nitrogen content and (a) Carter Index and (b) Lichtenthaler Index for N (filled red circles) and P (open blue circles) limited plants. Lines have been fitted to relationships that are significant at $P < 0.05$ with the red lines fitted to N limited data.

Using the N limited dataset, many other chlorophyll related indices were significantly related to N. A total of 12 indices were strongly related to N with $R^2 > 0.8$ and were modelled using a combination of linear and second order polynomial functions. The six indices that were most strongly related to N included Blue Red Pigment Index (Zarco-Tejada et al., 2005), Simple Ratio Pigment Index (Penuelas et al., 1995a), Normalised Pigment Chlorophyll Ratio Index (Peñuelas et al., 1994), Modified Normalised Difference, Red Edge Modified Normalised Difference Vegetation Index (Sims and Gamon, 2002) and PRI.

Models of P were markedly different when data were restricted to only P limited observations than relationships fitted to all data or N limited observations. Using all the data, P was most strongly predicted by Anthocyanin Reflectance Index $((1/R_{550}) - (1/R_{700}))$, Red Green Ratio Index (R_{690}/R_{550}) and Reciprocal Reflectance ($1/R_{700}$) and these linear relationships had respective R^2 of 0.31, 0.26 and 0.20. In contrast, when data was restricted to the P limited range only PRI and SIF were significantly related to P.

Table 2. Summary of statistics for models predicting area based nitrogen and phosphorus content from hyperspectral Indices and Solar-Induced Chlorophyll Fluorescence (SIF). The presented models use the entire dataset ($n = 60$) and both the N limited ($n = 43$) and the P limited dataset ($n = 17$). The two hyperspectral variables with the strongest relations to N and P are shown and the strength of these relationships is shown for predictions of both elements. Values shown include the RMSE and coefficient of determination (R^2) which is followed by the P category, in which asterisks ***, **, * represent significance at $P = 0.001$, 0.01 and 0.05 , respectively, and ns = non-significant at $P = 0.05$.

Variable	All data		N limiting		P limiting	
	R^2	RMSE	R^2	RMSE	R^2	RMSE
Prediction of N						
Carter Index	0.90***	3.86	0.89***	3.09	0.01 ^{ns}	3.32
Lichtenthaler Ind.	0.89***	4.01	0.88***	3.21	0.02 ^{ns}	3.29
PRI	0.76***	5.92	0.83***	3.82	0.05 ^{ns}	3.23
SIF	0.64***	7.16	0.57***	6.01	0.08 ^{ns}	3.19
Prediction of P						
PRI	0.08 ^{ns}	1.53	0.29***	1.45	0.75***	0.37
SIF	0.01 ^{ns}	1.59	0.09*	1.64	0.52**	0.52
Carter Index	0.04 ^{ns}	1.56	0.30***	1.45	0.14 ^{ns}	0.70
Lichtenthaler Ind.	0.02 ^{ns}	1.58	0.27***	1.48	0.05 ^{ns}	0.73

Using observations from the P limited dataset, PRI was most strongly related to P (blue circles, Fig. 6a) and this positive linear relationship had an R^2 of 0.75. In contrast, the relationship between P and PRI was markedly weaker using the N limited dataset ($R^2=0.29$; $P<0.001$) and all data ($R^2=0.08$; $P=0.03$) (Table 2). Similarly, SIF exhibited a linear relationship of moderate strength with P ($R^2=0.52$, $P <0.01$) using P limited data (Fig. 6b), which was markedly stronger than the relationships using N limited observations ($R^2=0.07$; $P=0.04$) or all data ($R^2=0.01$; $P=0.51$). Using analysis of covariance, the linear models fitted between P and both PRI and SIF for N limited plants had a significantly lower slope ($P<0.01$ for SIF and $P <0.001$ for PRI) and significantly higher intercept ($P<0.001$ for both PRI and SIF) than linear models fitted to P limited trees.

Both PRI and SIF were significantly related to N when data was constrained to the N limiting dataset (Table 2). The relationship between PRI and N was exponential (Fig. 6c) and accounted for 83% of the variance in the data while the relationship between SIF and N was linear (Fig. 6d) with R^2 of 0.57 (Table 2). Relationships between these two variables and N were insignificant using the P limited dataset (Table 2) and these data added considerable scatter to the regressions using N limited trees at high values of N (Figs. 6c, d). This was reflected by differences in RMSE which were markedly higher for all data than N limited data for relationships between N and both PRI (5.92 vs 3.82 $\mu\text{g cm}^{-2}$) and SIF (7.16 vs. 6.01 $\mu\text{g cm}^{-2}$).

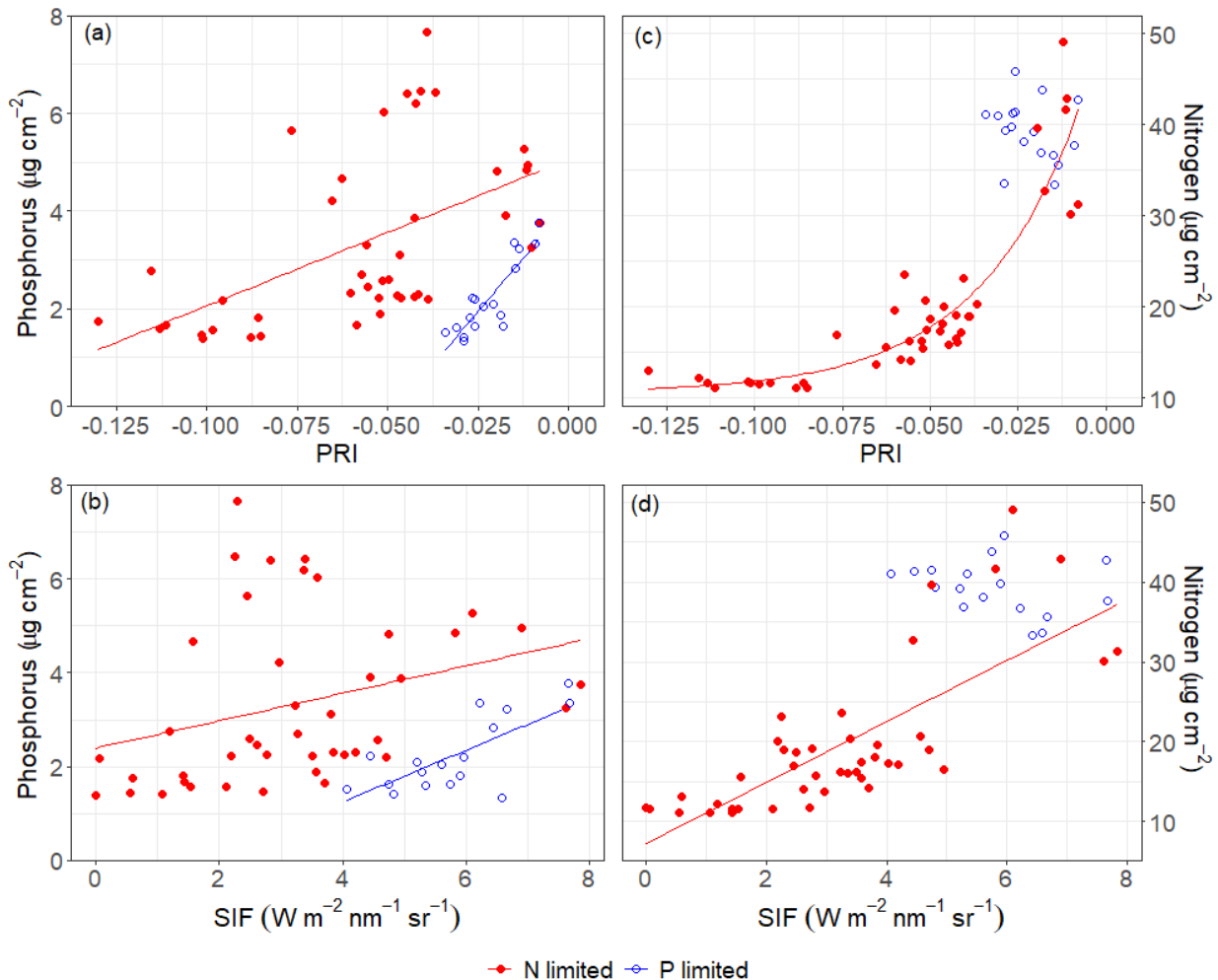


Figure 6. Relationships between phosphorus content and (a) Photochemical Reflectance Index (PRI) and (b) Solar-Induced Chlorophyll Fluorescence (SIF). Also shown are relationships between nitrogen and (c) PRI and (d) SIF. Data shown include trees grown under N (filled red circles) and P limiting conditions (open blue circles). Lines have been fitted to relationships that are significant at $P < 0.05$ with the red lines fitted to N limited data and blue lines fitted to P limited data.

3.6 Models of V_{cmax} and J_{max}

Predictions using SIF and PRI demonstrated that these variables could be used to estimate V_{cmax} and J_{max} using a single equation across both N and P limiting ranges (Fig. 7). Using all the data SIF exhibited strong positive linear relationships with both V_{cmax} ($R^2 = 0.78$; $P < 0.001$) and J_{max} ($R^2 = 0.80$; $P < 0.001$), which were slightly reduced in strength when data was restricted to N limiting measurements, to respective R^2 values of 0.69 and 0.77 (Fig. 7a, b). Under P limiting conditions, SIF was moderately related to V_{cmax} ($R^2 = 0.35$; $P = 0.09$) and strongly related to J_{max} ($R^2 = 0.68$; $P < 0.01$) and these relationships aligned very well with predictions made under N limiting conditions (Fig. 7a, b). Using P limited data, predictions of both V_{cmax} and J_{max} using SIF were of a similar strength to predictions made directly using P and markedly higher than predictions made using other indices (Fig. 8).

Using all the data there were strong relationships between PRI and both V_{cmax} ($R^2 = 0.83$; $P < 0.001$) and J_{max} ($R^2 = 0.83$; $P < 0.001$) that were best described using a quadratic relationship (Fig. 7c, d). These relationships remained strong, but the precision was slightly reduced when data was restricted to N limited measurements to respective R^2 values of 0.77 and 0.79 (Fig. 7c, d). Under P limiting conditions, positive correlations of moderate strength were found between PRI and V_{cmax} ($R^2 = 0.34$; $P = 0.10$) and J_{max} ($R^2 = 0.41$; $P = 0.06$), that were generally aligned with predictions under N limiting conditions (Fig. 7c, d). Although predictions under P limiting conditions using PRI were not as strong

as those that used SIF or P, these predictions were markedly more precise than those using other indices (Fig. 8).

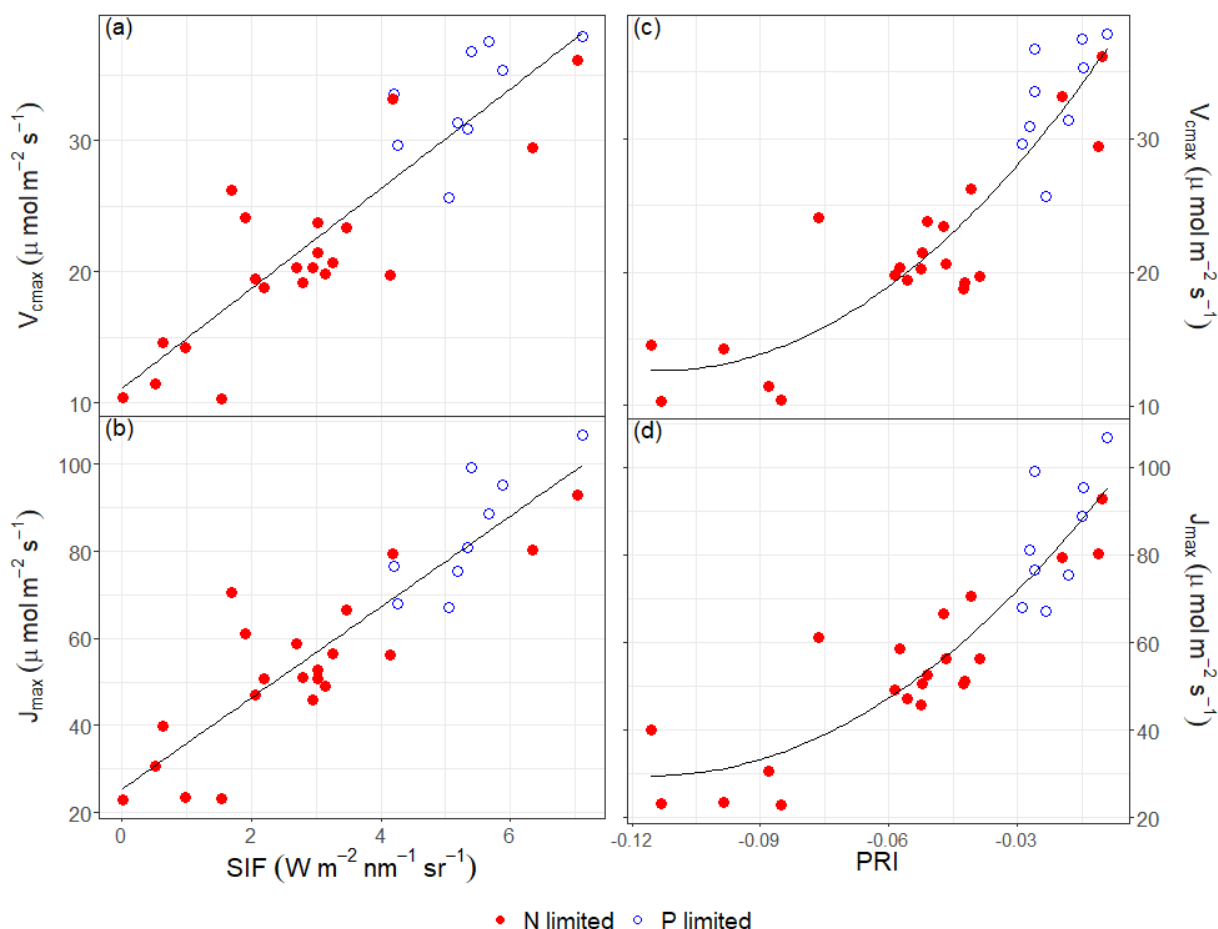


Figure 7. Relationships between Photochemical Reflectance Index and Solar-Induced Chlorophyll Fluorescence and (a, c) V_{cmax} and (b, d) J_{max} under N (filled red circles) and P limiting conditions (open blue circles). The black lines were fitted to both N and P limited data.

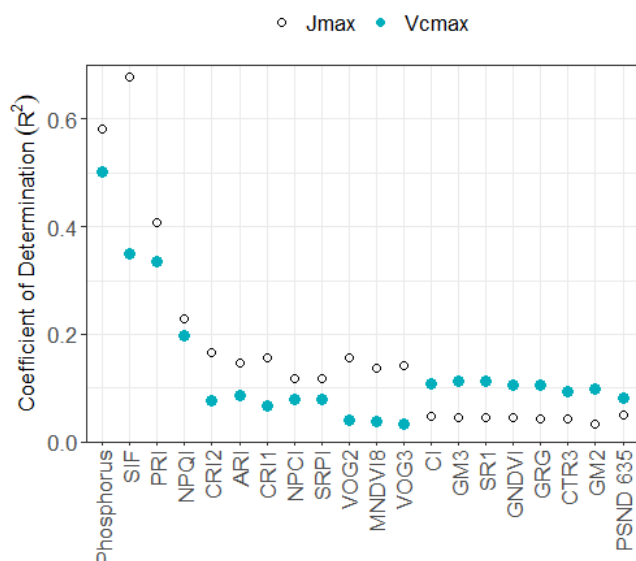


Figure 8. Coefficient of determination between V_{cmax} (filled teal circles), J_{max} (open black circles) and area based phosphorus, SIF, PRI, and 17 additional indices that were most strongly related to V_{cmax} and J_{max} . The relationships shown were constructed using P limited data and predictors are sorted in descending order of mean R^2 for V_{cmax} and J_{max} .

DISCUSSION

This study advances our understanding of the functional relationships between SIF, PRI and both foliage nutrition and photosynthesis. The strongest relationships between N and P and both V_{cmax} and J_{max} were developed through splitting the data at N/P =10 suggesting that photosynthesis is independently limited by these elements. The model that was used to accurately partition N from P limited trees demonstrated the importance of PRI and SIF in separating these two groups. Within each of these two limiting phases robust predictions of N and P were made using PRI and SIF. Although indices that were surrogates for chlorophyll were also useful for prediction of N these variables exhibited little correlation with P when data were restricted to the P limiting range. Through their correlations with N and P, both PRI and SIF were positively correlated to V_{cmax} and J_{max} and these relationships appeared to be generalisable across the N and P limiting ranges. Partitioning of data into N and P limited ranges revealed relationships between hyperspectral data, foliage nutrition and photosynthesis that were not evident using the unpartitioned dataset.

Our results support the premise that N and P independently limit photosynthesis. There were marked increases in the strength of relationships between P and both V_{cmax} and J_{max} as data was increasingly restricted from all measurements to data with N/P > 10. Although N was positively correlated to both V_{cmax} and J_{max} using all data, there were increases in the precision of these relationships when data was restricted to the N limiting range, particularly at N/P ≤ 5, but also at N/P ≤ 10. Further evidence that N independently limits photosynthesis was demonstrated by the lack of a significant correlation between N and either V_{cmax} and J_{max} when data was restricted to the P limiting range at N/P >10. Compared to these predictions using N, the use of P as a predictive variable for data with N/P > 10 markedly improved the strength of these correlations for both V_{cmax} ($R^2 = 0.50$ vs. 0.01) and J_{max} ($R^2 = 0.58$ vs. 0.02) strongly suggesting that there is a functional explanation for this uncorrelated scatter at high values of N.

Trees that were limited by N and P were accurately partitioned using PRI, SIF and three indices that were representative of differences in reflectance and photosynthesis between these two groups. Variable importance values show that group separation was primarily attributable to PRI and SIF. The separation of N and P limited trees by PRI and SIF into respectively, low and high values, reflects the higher rates of photosynthesis in P limited plants.

In contrast to previous research our predictions of P using all data were relatively weak. The precision of the strongest model of P using all data ($R^2 = 0.31$) was at the lower end of reported values for a range of species, which ranged from 0.32 to 0.95 (Asner and Martin, 2008; Asner et al., 2011; Curran et al., 2001; Gillon et al., 1999; Masaitis et al., 2014; Petisco et al., 2005; Stein et al., 2014), but was comparable to a previous study in *P. radiata* that utilised hyperspectral imagery from satellite (Sims et al., 2013). The poor precision of these models was expected as N and P were not significantly related. This feature of our dataset, in combination with partitioning of data into limiting ranges, revealed the key hyperspectral variables that were related to P.

When data were restricted to the P limited range, only SIF and PRI were significant predictors of P and these variables exhibited moderate to strong positive relationships with P. In contrast to other indices used in the analysis, which are mainly proxies for chlorophyll content, these two variables are plant related traits that are more directly linked to photosynthetic activity. The availability of P has an impact on many important aspects of photosynthesis (Marschner, 1995; Taiz et al., 2015) and, as shown in our study, P has been found to be significantly and positively related to both V_{cmax} and J_{max} (Bown et al., 2007). Given that photosynthetic rate is also positively related to both PRI (Gamon et al., 2016; Ripullone et al., 2011; Scholten et al., 2019; Wong and Gamon, 2015a, b) and SIF (Frankenberg et al., 2011; Guanter et al., 2014; Smith et al., 2018) it follows that these traits were positively related to P when data was restricted to the P limiting range.

Indices that were proxies for chlorophyll content were the strongest predictions of N. The most precise predictions of N were made using the Carter and Lichtenthaler indices which are similar formulations that characterise the extent of leftwards shift in the red edge that occurs in plants with lower chlorophyll content (Carter, 1994; Lichtenthaler et al., 1996). These indices accounted for 88-

89% of the variance in N which suggests that wavelengths associated with protein in the SWIR range are not as important for predicting N in *P. radiata* as those associated with chlorophyll in the VNIR range. Splitting the full dataset into the N limiting range did not markedly alter the R^2 of these relationships but did improve the RMSE which is a more sensitive indicator of model error. When data was restricted to the P limited range neither the Carter nor Lichtenthaler index were significantly related to N. This finding reinforces the importance of removing P limited data from these analyses to avoid adding scatter into predictions at high values of N.

Analyses show that PRI and SIF were the only two variables that could be used to predict both N and P with a reasonable degree of precision. The use of a N/P ratio to separate out the P limiting range allowed us to detect relationships between P and these two variables that were insignificant using all data. In contrast to proxies for chlorophyll, both PRI and SIF can account for variation in P, through their correlations with biochemical limitations to photosynthesis, which have a sound mechanistic basis.

SIF was strongly correlated with both V_{cmax} and J_{max} and predictions exhibited relatively robust correlations across both the N and P limiting ranges. Although SIF has been widely used to predict gross primary productivity (Meroni et al., 2009; Porcar-Castell et al., 2014; Rascher et al., 2015), and photosynthesis in a range of species (Frankenberg et al., 2011; Guanter et al., 2014; Smith et al., 2018), with few exceptions (Camino et al., 2019), little research has linked SIF to V_{cmax} and J_{max} at a fine scale. It has been hypothesised that SIF is a useful predictor of photosynthetic capacity as it can be used to selectively measure the quantity of absorbed light in chlorophyll (Rascher et al., 2015). Our results suggest that SIF can at least partially account for the role of P on photosynthetic capacity at high values of N as supported by the strong relationship found between SIF and P under P limiting conditions.

Similarly, PRI was also strongly related to photosynthetic capacity and was able to account for variation in V_{cmax} and J_{max} across both N and P limitations. Research has widely demonstrated the utility of PRI for predicting light use efficiency (Garbulsky et al., 2011; Peñuelas et al., 2011) and key photosynthetic parameters under a range of stresses including severe drought conditions (Ripullone et al., 2011), cold winter temperatures (Gamon et al., 2016; Wong and Gamon, 2015a, b) and herbicide damage (Scholten et al., 2019). The relationship found here between PRI and photosynthetic capacity is consistent with Scholten et al. (2019) and has a strong theoretical basis as PRI can track plant photosynthetic activity through its intimate link with the dissipation of excess energy by nonphotochemical quenching (NPQ) via the xanthophyll cycle (Gamon et al., 1997). The xanthophyll cycle is activated during periods of excess excitation energy in the leaf and through this process violaxanthin is de-epoxidized to zeaxanthin. These increased concentrations in zeaxanthin reduce reflectance at wavelengths around 531 nm, which results in reductions in PRI (Gamon et al., 1992; Peñuelas et al., 1995). As with SIF, our results suggest that PRI may provide a generalisable means of predicting photosynthetic capacity, through the correlation of this variable with both N and P, under a range of nutritional limitations. However, a detailed examination of the mechanistic links between photosynthesis, nutrition and both PRI and SIF was beyond the scope of this study. Further research is required to more fully understand the nature of these linkages.

The use of PRI and SIF to predict photosynthesis and foliage nutrition could be scaled up using hyperspectral imagery acquired from UAV, fixed wing aircraft or satellite. Both PRI and SIF can be determined using lightweight hyperspectral imagers (see review by Aasen et al., 2018) on board drones using linear-array imagers (Zarco-Tejada et al., 2012) with a limited number of spectral bands (Poblete et al., 2020). For large-scale monitoring purposes, the presented models could be used to monitor thousands of hectares using manned aircraft and commercial imaging spectrometers (Zarco-Tejada et al., 2018) including large facilities such as APEX (Damm et al., 2015). Currently there are a number of sophisticated aircraft-based platforms that allow capture of hyperspectral data (for summary see Watt et al., 2019) often in conjunction with other data sources (i.e. LiDAR, thermal). Sensors that can capture at a fine spectral resolution (≤ 5 nm) include Carnegie Airborne Observatory (CAO) and CAO-2 systems (Asner et al., 2012) G-LiHT (Cook et al., 2013) and the LiChy system (Pang et al., 2016).

As summarised in Mohammed et al. (2019) measurements of SIF are currently taken from a number of satellite platforms (e.g. GOME-2, OCO-2) and the first satellite mission designed for SIF measurement, FLEX, is scheduled for launch in 2022. The recently launched PRISMA, DESIS and HISUI hyperspectral imagers, and the EnMAP sensor, which is scheduled for launch in 2021, are particularly suitable for estimating PRI and will provide imagery at a spatial resolution of 30 m with a relatively fine spectral resolution of up to 6.5 nm within the VNIR range (Guanter et al., 2015). In addition, Sentinel-3 has been proposed for V_{cmax} estimation at global scales using radiative transfer models such as SCOPE (Prikaziuk and van der Tol, 2019).

Scaling up the methods presented here using lower resolution imagery acquired as part of large-scale monitoring campaigns will require appropriate radiative transfer modelling methods. These are needed to account for the structural, background and shadow effects typical of forest stands. A robust assessment of the physiological status of vegetation will require physical models to analyse the impacts of structural effects on the radiance and reflectance signal used to calculate the fluorescence emission and indices such as PRI.

In conclusion, this study shows that N and P independently pose biochemical limitations to photosynthesis and the most precise relationships between foliage nutrition and V_{cmax} and J_{max} were constructed using data partitioned at $N/P = 10$. Although the strongest models of N used indices that served as proxies for chlorophyll content these indices were not significantly related to P within the P limiting range. Using P limited data only PRI and SIF were significantly related to P and both of these variables were also robust predictors of N using N limited data as they are proxies for photosynthesis. Given the robust correlations of PRI and SIF with N and P, these variables were also precise predictors of V_{cmax} and J_{max} across both N and P limiting ranges. Separation of data into N and P limited groups provided insight into relationships that would have otherwise been concealed and demonstrate that more robust predictions of N and P and biochemical limitations to photosynthesis can be developed using this method. Further research should examine this approach for identifying N and P limitations and developing models that link hyperspectral data to nutrient content and photosynthesis at increased scale across a broader range of species.

CONCLUSIONS

In conclusion, this study shows that N and P independently pose biochemical limitations to photosynthesis and the most precise relationships between foliage nutrition and V_{cmax} and J_{max} were constructed using data partitioned at $N/P = 10$. Although the strongest models of N used indices that served as proxies for chlorophyll content these indices were not significantly related to P within the P limiting range. Using P limited data only PRI and SIF were significantly related to P and both of these variables were also robust predictors of N using N limited data as they are proxies for photosynthesis. Given the robust correlations of PRI and SIF with N and P, these variables were also precise predictors of V_{cmax} and J_{max} across both N and P limiting ranges. Separation of data into N and P limited groups provided insight into relationships that would have otherwise been concealed and demonstrate that more robust predictions of N and P and biochemical limitations to photosynthesis can be developed using this method. Further research should examine this approach for identifying N and P limitations and developing models that link hyperspectral data to nutrient content and photosynthesis at increased scale. A research project is already underway to extrapolate these findings to the accelerator trials using UAV acquired hyperspectral imagery.

ACKNOWLEDGEMENTS

We are grateful to Kendra Newick who assisted with the preparation of the nutrient solutions. The project was partly funded through the Resilient Forests programme, which is funded through Scion SSIF as well as the Forest Grower's Levy Trust. Funding was also received from the National Institute for Forest Products Innovation (Project Number NIF073-1819), which comprised contributions from the Australian Government, Australasian Forestry Companies and South Australian and Tasmanian State Governments.

REFERENCES

- Aasen, H., Honkavaara, E., Lucieer, A., Zarco-Tejada, P.J., 2018. Quantitative remote sensing at ultra-high resolution with UAV spectroscopy: a review of sensor technology, measurement procedures, and data correction workflows. *Remote Sensing* 10, 1091.
- Aerts, R., Chapin, F.S., 2000. The mineral nutrition of wild plants revisited: A re-evaluation of processes and patterns, *Advances in Ecological Research*, Vol 30, pp. 1-67.
- Akinwande, M.O., Dikko, H.G., Samson, A., 2015. Variance inflation factor: as a condition for the inclusion of suppressor variable (s) in regression analysis. *Open Journal of Statistics* 5, 754.
- Albaugh, T.J., Allen, H.L., Zutter, B.R., Quicke, H.E., 2003. Vegetation control and fertilization in midrotation *Pinus taeda* stands in the southeastern United States. *Ann Forest Sci* 60, 619-624.
- Allen, H.L., Fox, T.R., Campbell, R.G., 2005. What is ahead for intensive pine plantation silviculture in the south? *Southern Journal of Applied Forestry* 29, 62-69.
- Asner, G.P., Knapp, D.E., Boardman, J., Green, R.O., Kennedy-Bowdoin, T., Eastwood, M., Martin, R.E., Anderson, C., Field, C.B., 2012. Carnegie Airborne Observatory-2: Increasing science data dimensionality via high-fidelity multi-sensor fusion. *Remote Sensing of Environment* 124, 454-465.
- Asner, G.P., Martin, R.E., 2008. Spectral and chemical analysis of tropical forests: Scaling from leaf to canopy levels. *Remote Sensing of Environment* 112, 3958-3970.
- Asner, G.P., Martin, R.E., Knapp, D.E., Tupayachi, R., Anderson, C., Carranza, L., Martinez, P., Houcheime, M., Sinca, F., Weiss, P., 2011. Spectroscopy of canopy chemicals in humid tropical forests. *Remote Sensing of Environment* 115, 3587-3598.
- Baret, F., Houlès, V., Guerif, M., 2007. Quantification of plant stress using remote sensing observations and crop models: the case of nitrogen management. *Journal of Experimental Botany* 58, 869-880.
- Barnes, J., Balaguer, L., Manrique, E., Elvira, S., Davison, A., 1992. A reappraisal of the use of DMSO for the extraction and determination of chlorophylls a and b in lichens and higher plants. *Environmental and Experimental botany* 32, 85-100.
- Blackburn, G.A., 1998. Spectral indices for estimating photosynthetic pigment concentrations: a test using senescent tree leaves. *International Journal of Remote Sensing* 19, 657-675.
- Blakemore, L.C., Searl, P.L., Daly, B.K., 1987. Methods for chemical analysis of soils. NZ Soil Bureau Scientific Report 80, 21-45.
- Bown, H.E., Watt, M.S., Clinton, P.W., Mason, E.G., Richardson, B., 2007. Partitioning concurrent influences of nitrogen and phosphorus supply on photosynthetic model parameters of *Pinus radiata*. *Tree Physiology* 27, 335-344.
- Bown, H.E., Watt, M.S., Mason, E.G., Clinton, P.W., Whitehead, D., 2009. The influence of nitrogen and phosphorus supply and genotype on mesophyll conductance limitations to photosynthesis in *Pinus radiata*. *Tree Physiology* 29, 1143-1151.
- Broge, N.H., Leblanc, E., 2001. Comparing prediction power and stability of broadband and hyperspectral vegetation indices for estimation of green leaf area index and canopy chlorophyll density. *Remote sensing of environment* 76, 156-172.
- Buddenbaum, H., Stern, O., Paschmionka, B., Hass, E., Gattung, T., Stoffels, J., Hill, J., Werner, W., 2015. Using VNIR and SWIR field imaging spectroscopy for drought stress monitoring of beech seedlings. *International Journal of Remote Sensing* 36, 4590-4605.
- Buddenbaum, H., Watt, M.S., Scholten, R.C., Hill, J., 2019. Preprocessing Ground-Based Visible/Near Infrared Imaging Spectroscopy Data Affected by Smile Effects. *Sensors* 19, 1543.
- Calderón, R., Navas-Cortés, J.A., Lucena, C., Zarco-Tejada, P.J., 2013. High-resolution airborne hyperspectral and thermal imagery for early detection of *Verticillium* wilt of olive using fluorescence, temperature and narrow-band spectral indices. *Remote Sensing of Environment* 139, 231-245.
- Camino, C., Gonzalez-Dugo, V., Hernandez, P., Zarco-Tejada, P.J., 2019. Radiative transfer V_{cmax} estimation from hyperspectral imagery and SIF retrievals to assess photosynthetic

- performance in rainfed and irrigated plant phenotyping trials. *Remote Sensing of Environment*, 111186.
- Campion, J., 2008. The effects of mid-and late-rotation fertiliser application on tree growth and wood quality in softwood saw-timber stands: a critical review. *Southern Forests: a Journal of Forest Science* 70, 7-17.
- Carter, G.A., 1994. Ratios of leaf reflectances in narrow wavebands as indicators of plant stress. *Remote sensing* 15, 697-703.
- Cendrero-Mateo, M.P., Moran, M.S., Papuga, S.A., Thorp, K.R., Alonso, L., Moreno, J., Ponce-Campos, G., Rascher, U., Wang, G., 2015. Plant chlorophyll fluorescence: active and passive measurements at canopy and leaf scales with different nitrogen treatments. *Journal of experimental botany* 67, 275-286.
- Chen, J.M., 1996. Evaluation of vegetation indices and a modified simple ratio for boreal applications. *Canadian Journal of Remote Sensing* 22, 229-242.
- Cook, B.D., Nelson, R.F., Middleton, E.M., Morton, D.C., McCorkel, J.T., Masek, J.G., Ranson, K.J., Ly, V., Montesano, P.M., 2013. NASA Goddard's LiDAR, hyperspectral and thermal (G-LiHT) airborne imager. *Remote Sensing* 5, 4045-4066.
- Coops, N.C., Smith, M.L., Martin, M.E., Ollinger, S.V., 2003. Prediction of eucalypt foliage nitrogen content from satellite-derived hyperspectral data. *IEEE Transactions on Geoscience and Remote Sensing* 41, 1338-1346.
- Croft, H., Chen, J., Zhang, Y., 2014. The applicability of empirical vegetation indices for determining leaf chlorophyll content over different leaf and canopy structures. *Ecological Complexity* 17, 119-130.
- Curran, P.J., 1989. Remote sensing of foliar chemistry. *Remote sensing of Environment* 30, 271-278.
- Curran, P.J., Dungan, J.L., Peterson, D.L., 2001. Estimating the foliar biochemical concentration of leaves with reflectance spectrometry: testing the Kokaly and Clark methodologies. *Remote Sensing of Environment* 76, 349-359.
- Damm, A., Erler, A., Hillen, W., Meroni, M., Schaepman, M.E., Verhoef, W., Rascher, U., 2011. Modeling the impact of spectral sensor configurations on the FLD retrieval accuracy of sun-induced chlorophyll fluorescence. *Remote Sensing of Environment* 115, 1882-1892.
- Damm, A., Guanter, L., Paul-Limoges, E., Van der Tol, C., Hueni, A., Buchmann, N., Eugster, W., Ammann, C., Schaepman, M.E., 2015. Far-red sun-induced chlorophyll fluorescence shows ecosystem-specific relationships to gross primary production: An assessment based on observational and modeling approaches. *Remote Sensing of Environment* 166, 91-105.
- Dash, J., Curran, P.J., 2004. The MERIS terrestrial chlorophyll index.
- Datt, B., 1999. Visible/near infrared reflectance and chlorophyll content in Eucalyptus leaves. *International Journal of Remote Sensing* 20, 2741-2759.
- Daughtry, C., Walthall, C., Kim, M., De Colstoun, E.B., McMurtrey Iii, J., 2000. Estimating corn leaf chlorophyll concentration from leaf and canopy reflectance. *Remote sensing of Environment* 74, 229-239.
- Dechant, B., Cuntz, M., Vohland, M., Schulz, E., Doktor, D., 2017. Estimation of photosynthesis traits from leaf reflectance spectra: correlation to nitrogen content as the dominant mechanism. *Remote sensing of environment* 196, 279-292.
- Dobrowski, S.Z., Pushnik, J.C., Zarco-Tejada, P.J., Ustin, S.L., 2005. Simple reflectance indices track heat and water stress-induced changes in steady-state chlorophyll fluorescence at the canopy scale. *Remote Sensing of Environment* 97, 403-414.
- Domingues, T.F., Meir, P., Feldpausch, T.R., Saiz, G., Veenendaal, E.M., Schrodte, F., Bird, M., Djagbletey, G., Hien, F., Compaore, H., 2010. Co-limitation of photosynthetic capacity by nitrogen and phosphorus in West Africa woodlands. *Plant, Cell & Environment* 33, 959-980.
- Downham, R., Gavran, M., 2019. Australian plantation statistics 2019 update. Aust Gov Dep Agric Water Resour Canberra, Aust 12.
- Drolet, G.G., Middleton, E.M., Huemmrich, K.F., Hall, F.G., Amiro, B.D., Barr, A.G., Black, T.A., McCaughey, J.H., Margolis, H.A., 2008. Regional mapping of gross light-use efficiency using MODIS spectral indices. *Remote Sensing of Environment* 112, 3064-3078.
- Evans, J.R., 1989. Photosynthesis and nitrogen relationships in leaves of C3 plants. *Oecologia* 78, 9-19.

- Fox, T.R., Allen, H.L., Albaugh, T.J., Rubilar, R., Carlson, C.A., 2007. Tree nutrition and forest fertilization of pine plantations in the southern United States. *Southern Journal of Applied Forestry* 31, 5-11.
- Frankenberg, C., Butz, A., Toon, G.C., 2011. Disentangling chlorophyll fluorescence from atmospheric scattering effects in O2 A-band spectra of reflected sun-light. *Geophysical Research Letters* 38.
- Fuentes, D.A., Gamon, J.A., Cheng, Y., Claudio, H.C., Qiu, H.-I., Mao, Z., Sims, D.A., Rahman, A.F., Oechel, W., Luo, H., 2006. Mapping carbon and water vapor fluxes in a chaparral ecosystem using vegetation indices derived from AVIRIS. *Remote Sensing of Environment* 103, 312-323.
- Gamon, J., Penuelas, J., Field, C., 1992. A narrow-waveband spectral index that tracks diurnal changes in photosynthetic efficiency. *Remote Sensing of environment* 41, 35-44.
- Gamon, J., Serrano, L., Surfus, J.S., 1997. The photochemical reflectance index: an optical indicator of photosynthetic radiation use efficiency across species, functional types, and nutrient levels. *Oecologia* 112, 492-501.
- Gamon, J.A., Huemmrich, K.F., Wong, C.Y.S., Ensminger, I., Garrity, S., Hollinger, D.Y., Noormets, A., Peñuelas, J., 2016. A remotely sensed pigment index reveals photosynthetic phenology in evergreen conifers. *Proceedings of the National Academy of Sciences* 113, 13087-13092.
- Garbulsky, M.F., Peñuelas, J., Gamon, J., Inoue, Y., Filella, I., 2011. The photochemical reflectance index (PRI) and the remote sensing of leaf, canopy and ecosystem radiation use efficiencies: A review and meta-analysis. *Remote sensing of environment* 115, 281-297.
- Gillon, D., Houssard, C., Joffre, R., 1999. Using near-infrared reflectance spectroscopy to predict carbon, nitrogen and phosphorus content in heterogeneous plant material. *Oecologia* 118, 173-182.
- Gitelson, A., Merzlyak, M.N., 1994. Spectral reflectance changes associated with autumn senescence of *Aesculus hippocastanum* L. and *Acer platanoides* L. leaves. Spectral features and relation to chlorophyll estimation. *Journal of Plant Physiology* 143, 286-292.
- Gitelson, A.A., Buschmann, C., Lichtenthaler, H.K., 1999. The chlorophyll fluorescence ratio F735/F700 as an accurate measure of the chlorophyll content in plants. *Remote Sensing of Environment* 69, 296-302.
- Gitelson, A.A., Gritz, Y., Merzlyak, M.N., 2003. Relationships between leaf chlorophyll content and spectral reflectance and algorithms for non-destructive chlorophyll assessment in higher plant leaves. *Journal of plant physiology* 160, 271-282.
- Gitelson, A.A., Kaufman, Y.J., Merzlyak, M.N., 1996. Use of a green channel in remote sensing of global vegetation from EOS-MODIS. *Remote Sensing Of Environment* 58, 289-298.
- Gitelson, A.A., Kaufman, Y.J., Stark, R., Rundquist, D., 2002a. Novel algorithms for remote estimation of vegetation fraction. *Remote sensing of Environment* 80, 76-87.
- Gitelson, A.A., Merzlyak, M.N., 1996. Signature analysis of leaf reflectance spectra: algorithm development for remote sensing of chlorophyll. *Journal of plant physiology* 148, 494-500.
- Gitelson, A.A., Merzlyak, M.N., 1997. Remote estimation of chlorophyll content in higher plant leaves. *International Journal of Remote Sensing* 18, 2691-2697.
- Gitelson, A.A., Merzlyak, M.N., Chivkunova, O.B., 2001. Optical properties and nondestructive estimation of anthocyanin content in plant leaves. *Photochemistry and photobiology* 74, 38-45.
- Gitelson, A.A., Zur, Y., Chivkunova, O.B., Merzlyak, M.N., 2002b. Assessing Carotenoid Content in Plant Leaves with Reflectance Spectroscopy. *Photochemistry and photobiology* 75, 272-281.
- Guan, L., Liu, X., 2009. Hyperspectral recognition models for physiological ecology characterization of rice in Cd pollution stress. *Ecology and Environmental Sciences* 18, 488-493.
- Guanter, L., Kaufmann, H., Segl, K., Foerster, S., Rogass, C., Chabrilat, S., Kuester, T., Hollstein, A., Rossner, G., Chlebek, C., 2015. The EnMAP spaceborne imaging spectroscopy mission for earth observation. *Remote Sensing* 7, 8830-8857.
- Guanter, L., Zhang, Y., Jung, M., Joiner, J., Voigt, M., Berry, J.A., Frankenberg, C., Huete, A.R., Zarco-Tejada, P., Lee, J.-E., 2014. Global and time-resolved monitoring of crop

- photosynthesis with chlorophyll fluorescence. *Proceedings of the National Academy of Sciences* 111, E1327-E1333.
- Guo, J., Trotter, C.M., 2004. Estimating photosynthetic light-use efficiency using the photochemical reflectance index: variations among species. *Functional Plant Biology* 31, 255-265.
- Haboudane, D., Miller, J.R., Pattey, E., Zarco-Tejada, P.J., Strachan, I.B., 2004. Hyperspectral vegetation indices and novel algorithms for predicting green LAI of crop canopies: Modeling and validation in the context of precision agriculture. *Remote sensing of environment* 90, 337-352.
- Haboudane, D., Miller, J.R., Tremblay, N., Zarco-Tejada, P.J., Dextraze, L., 2002. Integrated narrow-band vegetation indices for prediction of crop chlorophyll content for application to precision agriculture. *Remote sensing of environment* 81, 416-426.
- Hernández-Clemente, R., Navarro-Cerrillo, R.M., Suárez, L., Morales, F., Zarco-Tejada, P.J., 2011. Assessing structural effects on PRI for stress detection in conifer forests. *Remote Sensing of Environment* 115, 2360-2375.
- Hilker, T., Coops, N.C., Hall, F.G., Black, T.A., Chen, B., Krishnan, P., Wulder, M.A., Sellers, P.J., Middleton, E.M., Huemrich, K.F., 2008. A modeling approach for upscaling gross ecosystem production to the landscape scale using remote sensing data. *Journal of Geophysical Research: Biogeosciences* 113.
- Hill, J., Buddenbaum, H., Townsend, P.A., 2019. Imaging Spectroscopy of Forest Ecosystems: Perspectives for the Use of Space-borne Hyperspectral Earth Observation Systems. *Surveys in Geophysics* 40, 553-588.
- Huang, Z., Turner, B.J., Dury, S.J., Wallis, I.R., Foley, W.J., 2004. Estimating foliage nitrogen concentration from HYMAP data using continuum removal analysis. *Remote Sensing of Environment* 93, 18-29.
- Huete, A., Liu, H., Batchily, K., Van Leeuwen, W., 1997. A comparison of vegetation indices over a global set of TM images for EOS-MODIS. *Remote sensing of environment* 59, 440-451.
- Ingestad, T., 1971. A definition of optimum nutrient requirements in Birch Seedlings. II. *Physiologia Plantarum* 24, 118-125.
- Ingestad, T., 1979. Mineral nutrient requirements of *Pinus silvestris* and *Picea abies* seedlings. *Physiologia Plantarum* 45, 373-380.
- Ingestad, T., Lund, A., 1986. New concepts on soil fertility and plant nutrition as illustrated by research on forest trees and stands. *Geoderma* 40, 237-252.
- Jordan, C.F., 1969. Derivation of leaf-area index from quality of light on the forest floor. *Ecology* 50, 663-666.
- Kattenborn, T., Schiefer, F., Zarco-Tejada, P., Schmidlein, S., 2019. Advantages of retrieving pigment content [$\mu\text{g}/\text{cm}^2$] versus concentration [%] from canopy reflectance. *Remote Sensing of Environment* 230, 111195.
- Kim, M.S., Daughtry, C., Chappelle, E., McMurtrey, J., Walthall, C., 1994. The use of high spectral resolution bands for estimating absorbed photosynthetically active radiation (A par).
- Knecht, M.F., Göransson, A., 2004. Terrestrial plants require nutrients in similar proportions. *Tree physiology* 24, 447-460.
- Knyazikhin, Y., Schull, M.A., Stenberg, P., Möttus, M., Rautiainen, M., Yang, Y., Marshak, A., Carmona, P.L., Kaufmann, R.K., Lewis, P., 2013. Hyperspectral remote sensing of foliar nitrogen content. *Proceedings of the National Academy of Sciences* 110, E185-E192.
- Kokaly, R.F., 2001. Investigating a physical basis for spectroscopic estimates of leaf nitrogen concentration. *Remote Sensing of Environment* 75, 153-161.
- Kokaly, R.F., Asner, G.P., Ollinger, S.V., Martin, M.E., Wessman, C.A., 2009. Characterizing canopy biochemistry from imaging spectroscopy and its application to ecosystem studies. *Remote Sensing of Environment* 113, S78-S91.
- Lewis, N.B., Ferguson, I.S., 1993. *Management of radiata pine*. Inkata Press, Melbourne.
- Liaw, A., Wiener, M., 2002. Classification and regression by randomForest. *R news* 2, 18-22.
- Lichtenthaler, H., Lang, M., Sowinska, M., Heisel, F., Miehe, J., 1996. Detection of vegetation stress via a new high resolution fluorescence imaging system. *Journal of plant physiology* 148, 599-612.
- Liechty, H.O., Fristoe, C., 2013. Response of Midrotation Pine Stands to Fertilizer and Herbicide Application in the Western Gulf Coastal Plain. *Southern Journal of Applied Forestry* 37, 69-74.

- Liu, J., Moore, J.M., 1990. Hue image RGB colour composition. A simple technique to suppress shadow and enhance spectral signature. *International Journal of Remote Sensing* 11, 1521-1530.
- Long, S.P., Bernacchi, C.J., 2003. Gas exchange measurements, what can they tell us about the underlying limitations to photosynthesis? Procedures and sources of error. *Journal of Experimental Botany* 54, 2393-2401.
- Luther, J.E., Carroll, A.L., 1999. Development of an index of balsam fir vigor by foliar spectral reflectance. *Remote sensing of Environment* 69, 241-252.
- Maccioni, A., Agati, G., Mazzinghi, P., 2001. New vegetation indices for remote measurement of chlorophylls based on leaf directional reflectance spectra. *Journal of Photochemistry and Photobiology B: Biology* 61, 52-61.
- Marschner, H., 1995. Mineral nutrition of higher plants, 2nd ed. Academic Press, London.
- Martin, M.E., Plourde, L.C., Ollinger, S.V., Smith, M.L., McNeil, B.E., 2008. A generalizable method for remote sensing of canopy nitrogen across a wide range of forest ecosystems. *Remote Sensing of Environment* 112, 3511-3519.
- Martin, R.E., Asner, G.P., Francis, E., Ambrose, A., Baxter, W., Das, A.J., Vaughn, N.R., Paz-Kagan, T., Dawson, T., Nydick, K., 2018a. Remote measurement of canopy water content in giant sequoias (*Sequoiadendron giganteum*) during drought. *Forest ecology and management* 419, 279-290.
- Martin, R.E., Chadwick, K.D., Brodrick, P.G., Carranza-Jimenez, L., Vaughn, N.R., Asner, G.P., 2018b. An approach for foliar trait retrieval from airborne imaging spectroscopy of tropical forests. *Remote Sensing* 10, 199.
- Masaitis, G., Mozgeris, G., Augustaitis, A., 2014. Estimating crown defoliation and the chemical constituents in needles of Scots pine (*Pinus sylvestris* L.) trees by laboratory acquired hyperspectral data. *Balt. For* 20, 314-325.
- McMurtrey Iii, J., Chappelle, E.W., Kim, M., Meisinger, J., Corp, L., 1994. Distinguishing nitrogen fertilization levels in field corn (*Zea mays* L.) with actively induced fluorescence and passive reflectance measurements. *Remote Sensing of Environment* 47, 36-44.
- McNeil, B.E., de Beurs, K.M., Eshleman, K.N., Foster, J.R., Townsend, P.A., 2007a. Maintenance of ecosystem nitrogen limitation by ephemeral forest disturbance: An assessment using MODIS, Hyperion, and Landsat ETM+. *Geophysical Research Letters* 34.
- McNeil, B.E., Read, J.M., Driscoll, C.T., 2007b. Foliar nitrogen responses to elevated atmospheric nitrogen deposition in nine temperate forest canopy species. *Environmental science & technology* 41, 5191-5197.
- Meroni, M., Rossini, M., Guanter, L., Alonso, L., Rascher, U., Colombo, R., Moreno, J., 2009. Remote sensing of solar-induced chlorophyll fluorescence: Review of methods and applications. *Remote Sensing of Environment* 113, 2037-2051.
- Merton, R., 1998. Monitoring community hysteresis using spectral shift analysis and the red-edge vegetation stress index, *Proceedings of the Seventh Annual JPL Airborne Earth Science Workshop*, pp. 12-16.
- Middleton, E.M., Cheng, Y.-B., Hilker, T., Black, T.A., Krishnan, P., Coops, N.C., Huemmrich, K.F., 2009. Linking foliage spectral responses to canopy-level ecosystem photosynthetic light-use efficiency at a Douglas-fir forest in Canada. *Canadian Journal of Remote Sensing* 35, 166-188.
- Mohammed, G.H., Colombo, R., Middleton, E.M., Rascher, U., van der Tol, C., Nedbal, L., Goulas, Y., Pérez-Priego, O., Damm, A., Meroni, M., 2019. Remote sensing of solar-induced chlorophyll fluorescence (SIF) in vegetation: 50 years of progress. *Remote sensing of environment* 231, 111177.
- Mouazen, A.M., Kuang, B., De Baerdemaeker, J., Ramon, H., 2010. Comparison among principal component, partial least squares and back propagation neural network analyses for accuracy of measurement of selected soil properties with visible and near infrared spectroscopy. *Geoderma* 158, 23-31.
- Mutanga, O., Skidmore, A.K., 2004. Narrow band vegetation indices overcome the saturation problem in biomass estimation. *International journal of remote sensing* 25, 3999-4014.
- Nichol, C.J., Huemmrich, K.F., Black, T.A., Jarvis, P.G., Walthall, C.L., Grace, J., Hall, F.G., 2000. Remote sensing of photosynthetic-light-use efficiency of boreal forest. *Agricultural and Forest Meteorology* 101, 131-142.

- Niinemets, Ü., Tenhunen, J.D., 1997. A model separating leaf structural and physiological effects on carbon gain along light gradients for the shade-tolerant species *Acer saccharum*. *Plant, Cell & Environment* 20, 845-866.
- NZFOA, 2018. 2018 Facts and Figures. New Zealand Plantation Forest Industry. New Zealand Forest Owners Association, Wellington, 35 pp.
- Ollinger, S.V., Richardson, A.D., Martin, M.E., Hollinger, D.Y., Frohling, S.E., Reich, P.B., Plourde, L.C., Katul, G.G., Munger, J.W., Oren, R., 2008. Canopy nitrogen, carbon assimilation, and albedo in temperate and boreal forests: Functional relations and potential climate feedbacks. *Proceedings of the National Academy of Sciences* 105, 19336-19341.
- Oppelt, N., Mauser, W., 2004. Hyperspectral monitoring of physiological parameters of wheat during a vegetation period using AVIS data. *International Journal of Remote Sensing* 25, 145-159.
- Pang, Y., Li, Z., Ju, H., Lu, H., Jia, W., Si, L., Guo, Y., Liu, Q., Li, S., Liu, L., 2016. LiCHy: The CAF's LiDAR, CCD and hyperspectral integrated airborne observation system. *Remote Sensing* 8, 398.
- Peñuelas, J., Baret, F., Filella, I., 1995a. Semi-empirical indices to assess carotenoids/chlorophyll a ratio from leaf spectral reflectance. *Photosynthetica* 31, 221-230.
- Peñuelas, J., Filella, I., Gamon, J.A., 1995b. Assessment of photosynthetic radiation-use efficiency with spectral reflectance. *New Phytologist* 131, 291-296.
- Peñuelas, J., Filella, I., Gamon, J.A., 1995. Assessment of photosynthetic radiation-use efficiency with spectral reflectance. *New Phytologist* 131, 291-296.
- Peñuelas, J., Gamon, J., Fredeen, A., Merino, J., Field, C., 1994. Reflectance indices associated with physiological changes in nitrogen- and water-limited sunflower leaves. *Remote sensing of Environment* 48, 135-146.
- Peñuelas, J., Garbalsky, M.F., Filella, I., 2011. Photochemical reflectance index (PRI) and remote sensing of plant CO₂ uptake. *New Phytologist* 191, 596-599.
- Petisco, C., García-Criado, B., De Aldana, B.R.V., Zabalgoceazcoa, I., Mediavilla, S., 2005. Use of near-infrared reflectance spectroscopy in predicting nitrogen, phosphorus and calcium contents in heterogeneous woody plant species. *Analytical and bioanalytical chemistry* 382, 458-465.
- Plascyk, J.A., 1975. The MK II Fraunhofer line discriminator (FLD-II) for airborne and orbital remote sensing of solar-stimulated luminescence. *Optical Engineering* 14, 144339.
- Poblete, T., Camino, C., Beck, P.S.A., Hornero, A., Kattenborn, T., Saponari, M., Boscia, D., Navas-Cortes, J.A., Zarco-Tejada, P.J., 2020. Detection of *Xylella fastidiosa* infection symptoms with airborne multispectral and thermal imagery: Assessing bandset reduction performance from hyperspectral analysis. *ISPRS Journal of Photogrammetry and Remote Sensing* 162, 27-40.
- Porcar-Castell, A., Tyystjärvi, E., Atherton, J., Van der Tol, C., Flexas, J., Pfündel, E.E., Moreno, J., Frankenberg, C., Berry, J.A., 2014. Linking chlorophyll a fluorescence to photosynthesis for remote sensing applications: mechanisms and challenges. *Journal of experimental botany* 65, 4065-4095.
- Porder, S., Asner, G.P., Vitousek, P.M., 2005. Ground-based and remotely sensed nutrient availability across a tropical landscape. *Proceedings of the National Academy of Sciences* 102, 10909-10912.
- Prikaziuk, E., van der Tol, C., 2019. Global Sensitivity Analysis of the SCOPE Model in Sentinel-3 Bands: Thermal Domain Focus. *Remote Sensing* 11, 2424.
- Qi, J., Chehbouni, A., Huete, A., Kerr, Y., Sorooshian, S., 1994. A modified soil adjusted vegetation index. *Remote sensing of environment* 48, 119-126.
- R Development Core Team, 2011. R: A language and environment for statistical computing. R Foundation for Statistical Computing, Vienna, Austria.
- Raison, R.J., Myers, B.J., 1992. The Biology of Forest Growth experiment : linking water and nitrogen availability to the growth of *Pinus radiata*, *Forest Ecology and Management*.
- Rascher, U., Alonso, L., Burkart, A., Cilia, C., Cogliati, S., Colombo, R., Damm, A., Drusch, M., Guanter, L., Hanus, J., 2015. Sun-induced fluorescence—a new probe of photosynthesis: First maps from the imaging spectrometer HyPlant. *Global change biology* 21, 4673-4684.
- Reich, P.B., Schoettle, A.W., 1988. Role of phosphorus and nitrogen in photosynthetic and whole plant carbon gain and nutrient use efficiency in eastern white pine. *Oecologia* 77, 25-33.

- Ripullone, F., Rivelli, A.R., Baraldi, R., Guarini, R., Guerrieri, R., Magnani, F., Peñuelas, J., Raddi, S., Borghetti, M., 2011. Effectiveness of the photochemical reflectance index to track photosynthetic activity over a range of forest tree species and plant water statuses. *Functional Plant Biology* 38, 177-186.
- Rock, B.N., Hoshizaki, T., Miller, J.R., 1988. Comparison of in situ and airborne spectral measurements of the blue shift associated with forest decline. *Remote Sensing of Environment* 24, 109-127.
- Rondeaux, G., Steven, M., Baret, F., 1996. Optimization of soil-adjusted vegetation indices. *Remote sensing of environment* 55, 95-107.
- Roujean, J.-L., Breon, F.-M., 1995. Estimating PAR absorbed by vegetation from bidirectional reflectance measurements. *Remote Sensing of Environment* 51, 375-384.
- Rouse Jr, J.W., Haas, R., Schell, J., Deering, D., 1974. Monitoring vegetation systems in the Great Plains with ERTS. NASA special publication 351, 309.
- Salas, C., Donoso, P.J., Vargas, R., Arriagada, C.A., Pedraza, R., Soto, D.P., 2016. The forest sector in Chile: an overview and current challenges. *Journal of Forestry* 114, 562-571.
- Schlerf, M., Atzberger, C., Hill, J., Buddenbaum, H., Werner, W., Schüller, G., 2010. Retrieval of chlorophyll and nitrogen in Norway spruce (*Picea abies* L. Karst.) using imaging spectroscopy. *International Journal of Applied Earth Observation and Geoinformation* 12, 17-26.
- Scholten, R.C., Hill, J., Werner, W., Buddenbaum, H., Dash, J.P., Gallego, M.G., Rolando, C.A., Pearse, G.D., Hartley, R., Estarija, H.J., 2019. Hyperspectral VNIR-spectroscopy and imagery as a tool for monitoring herbicide damage in wilding conifers. *Biological Invasions* 21, 3395-3413.
- Serbin, S.P., Singh, A., McNeil, B.E., Kingdon, C.C., Townsend, P.A., 2014. Spectroscopic determination of leaf morphological and biochemical traits for northern temperate and boreal tree species. *Ecological Applications* 24, 1651-1669.
- Sheriff, D.W., Nambiar, E.K.S., Fife, D.N., 1986. Relationships between nutrient status, carbon assimilation and water use efficiency in *Pinus radiata* (D. Don) needles. *Tree Physiology* 2, 73-88.
- Sims, D.A., Gamon, J.A., 2002. Relationships between leaf pigment content and spectral reflectance across a wide range of species, leaf structures and developmental stages. *Remote sensing of environment* 81, 337-354.
- Sims, N.C., Culvenor, D., Newnham, G., Coops, N.C., Hopmans, P., 2013. Towards the operational use of satellite hyperspectral image data for mapping nutrient status and fertilizer requirements in Australian plantation forests. *IEEE Journal of Selected Topics in Applied Earth Observations and Remote Sensing* 6, 320-328.
- Singh, A., Serbin, S.P., McNeil, B.E., Kingdon, C.C., Townsend, P.A., 2015. Imaging spectroscopy algorithms for mapping canopy foliar chemical and morphological traits and their uncertainties. *Ecological Applications* 25, 2180-2197.
- Smith, M.L., Martin, M.E., Plourde, L., Ollinger, S.V., 2003. Analysis of hyperspectral data for estimation of temperate forest canopy nitrogen concentration: comparison between an airborne (AVIRIS) and a spaceborne (Hyperion) sensor. *IEEE Transactions on Geoscience and Remote Sensing* 41, 1332-1337.
- Smith, W.K., Biederman, J.A., Scott, R.L., Moore, D.J.P., He, M., Kimball, J.S., Yan, D., Hudson, A., Barnes, M.L., MacBean, N., 2018. Chlorophyll fluorescence better captures seasonal and interannual gross primary productivity dynamics across dryland ecosystems of southwestern North America. *Geophysical Research Letters* 45, 748-757.
- Stein, B.R., Thomas, V.A., Lorentz, L.J., Strahm, B.D., 2014. Predicting macronutrient concentrations from loblolly pine leaf reflectance across local and regional scales. *GIScience & remote sensing* 51, 269-287.
- Stylinski, C.D., Oechel, W.C., Gamon, J.A., Tissue, D.T., Miglietta, F., Raschi, A., 2000. Effects of lifelong [CO₂] enrichment on carboxylation and light utilization of *Quercus pubescens* Willd. examined with gas exchange, biochemistry and optical techniques. *Plant, Cell & Environment* 23, 1353-1362.
- Suarez, L., Zarco-Tejada, P.J., Sepulcre-Canto, G., Perez-Priego, O., Miller, J.R., Jimenez-Munoz, J.C., Sobrino, J., 2008. Assessing canopy PRI for water stress detection with diurnal airborne imagery. *Remote Sensing Of Environment* 112, 560-575.

- Taiz, L., Zeiger, E., Møller, I.M., Murphy, A., 2015. Plant physiology and development.
- Townsend, P.A., Foster, J.R., Chastain, R.A., Currie, W.S., 2003. Application of imaging spectroscopy to mapping canopy nitrogen in the forests of the central Appalachian Mountains using Hyperion and AVIRIS. *IEEE Transactions on Geoscience and Remote Sensing* 41, 1347-1354.
- Tsay, M.-L., Gjerstad, D.H., Glover, G.R., 1982. Tree leaf reflectance: a promising technique to rapidly determine nitrogen and chlorophyll content. *Canadian Journal of Forest Research* 12, 788-792.
- Vasques, G.M., Grunwald, S., Sickman, J.O., 2008. Comparison of multivariate methods for inferential modeling of soil carbon using visible/near-infrared spectra. *Geoderma* 146, 14-25.
- Vogelmann, J., Rock, B., Moss, D., 1993. Red edge spectral measurements from sugar maple leaves. *Remote Sensing* 14, 1563-1575.
- Walker, A.P., Beckerman, A.P., Gu, L., Kattge, J., Cernusak, L.A., Domingues, T.F., Scales, J.C., Wohlfahrt, G., Wullschlegel, S.D., Woodward, F.I., 2014. The relationship of leaf photosynthetic traits— V_{cmax} and J_{max} —to leaf nitrogen, leaf phosphorus, and specific leaf area: a meta-analysis and modeling study. *Ecology and evolution* 4, 3218-3235.
- Wang, Z., Skidmore, A.K., Darvishzadeh, R., Wang, T., 2018. Mapping forest canopy nitrogen content by inversion of coupled leaf-canopy radiative transfer models from airborne hyperspectral imagery. *Agricultural and forest meteorology* 253, 247-260.
- Wang, Z., Skidmore, A.K., Wang, T., Darvishzadeh, R., Hearne, J., 2015. Applicability of the PROSPECT model for estimating protein and cellulose+ lignin in fresh leaves. *Remote sensing of environment* 168, 205-218.
- Watt, M.S., Coker, G., Clinton, P.W., Davis, M.R., Parfitt, R., Simcock, R., Garret, L., Payn, T.W., Richardson, B., Dunningham, A., 2005. Defining sustainability of plantation forests through identification of site quality indicators influencing productivity- a national view for New Zealand. *Forest Ecology and Management* 216, 51-63.
- Watt, M.S., Pearse, G.D., Dash, J.P., Melia, N., Leonardo, E.M.C., 2019. Application of remote sensing technologies to identify impacts of nutritional deficiencies on forests. *ISPRS Journal of Photogrammetry and Remote Sensing* 149, 226-241.
- Wong, C.Y.S., Gamon, J.A., 2015a. The photochemical reflectance index provides an optical indicator of spring photosynthetic activation in evergreen conifers. *New Phytologist* 206, 196-208.
- Wong, C.Y.S., Gamon, J.A., 2015b. Three causes of variation in the photochemical reflectance index (PRI) in evergreen conifers. *New Phytologist* 206, 187-195.
- Wu, C., Niu, Z., Tang, Q., Huang, W., 2008. Estimating chlorophyll content from hyperspectral vegetation indices: Modeling and validation. *Agricultural and Forest Meteorology* 148, 1230-1241.
- Yoder, B.J., Pettigrew-Crosby, R.E., 1995. Predicting nitrogen and chlorophyll content and concentrations from reflectance spectra (400–2500 nm) at leaf and canopy scales. *Remote sensing of environment* 53, 199-211.
- Zarco-Tejada, P.J., Berjón, A., López-Lozano, R., Miller, J.R., Martín, P., Cachorro, V., González, M., De Frutos, A., 2005. Assessing vineyard condition with hyperspectral indices: Leaf and canopy reflectance simulation in a row-structured discontinuous canopy. *Remote Sensing of Environment* 99, 271-287.
- Zarco-Tejada, P.J., Catalina, A., González, M.R., Martín, P., 2013. Relationships between net photosynthesis and steady-state chlorophyll fluorescence retrieved from airborne hyperspectral imagery. *Remote Sensing of Environment* 136, 247-258.
- Zarco-Tejada, P.J., González-Dugo, M.V., Fereres, E., 2016. Seasonal stability of chlorophyll fluorescence quantified from airborne hyperspectral imagery as an indicator of net photosynthesis in the context of precision agriculture. *Remote Sensing of Environment* 179, 89-103.
- Zarco-Tejada, P.J., González-Dugo, V., Berni, J.A.J., 2012. Fluorescence, temperature and narrow-band indices acquired from a UAV platform for water stress detection using a micro-hyperspectral imager and a thermal camera. *Remote sensing of environment* 117, 322-337.

- Zarco-Tejada, P.J., Miller, J.R., Mohammed, G., Noland, T.L., Sampson, P., 1999. Canopy optical indices from infinite reflectance and canopy reflectance models for forest condition monitoring: Application to hyperspectral CASI data, IEEE 1999 International Geoscience and Remote Sensing Symposium. IGARSS'99 (Cat. No. 99CH36293). IEEE, pp. 1878-1881.
- Zarco-Tejada, P.J., Miller, J.R., Noland, T.L., Mohammed, G.H., Sampson, P.H., 2001. Scaling-up and model inversion methods with narrowband optical indices for chlorophyll content estimation in closed forest canopies with hyperspectral data. IEEE Transactions on Geoscience and Remote Sensing 39, 1491-1507.

Appendix 1. Summary of Indices used within this study.

Index	Full name	Equation	Reference
ARI	Anthocyanin Reflectance Index	$(1/R550) - (1/R700)$	Gitelson et al. (2001)
BGI1	Blue green pigment index	$R400/R550$	Zarco-Tejada et al. (2005)
BGI2	Blue green pigment index	$R450/R550$	Zarco-Tejada et al. (2005)
BRI1	Blue red pigment index	$R400/R690$	Zarco-Tejada et al. (2005)
BRI2	Blue red pigment index	$R450/R690$	Zarco-Tejada et al. (2005)
CARI	Chlorophyll absorption ratio index	$(R700 - R670) - (0.2 \times (R700 - R550))$	Kim et al. (1994)
CI	Colouration index	$(R800 - R550)/R800$	Liu and Moore (1990)
CR11	Carotenoid Reflectance Index	$(1/R510) - (1/R550)$	Gitelson et al. (2002b)
CR12	Carotenoid Reflectance Index 2	$(1/R510) - (1/R700)$	Gitelson et al. (2002b)
CTR1	Carter Index 1	$R695/R420$	Carter (1994)
CTR2	Carter Index 2	$R695/R760$	Carter (1994)
CTR3	Carter Index 3	$R605/R760$	Carter (1994)
CTR4	Carter Index 4	$R710/R760$	Carter (1994)
CTR5	Carter Index 5	$R695/R670$	Carter (1994)
CUR	Curvature index	$(R675 \times R690)/R683^2$	Zarco-Tejada et al. (2001)
Datt99	Datt, 99	$(R850 - R710)/(R850 - R680)$	Datt (1999)
Datt1	Maccioni, 2001	$(R780 - R710)/(R780 - R680)$	Maccioni et al. (2001)
DVI	Difference vegetation index	$R800 - R680$	Jordan (1969)
EVI	Enhanced vegetation index	$2.5 \times ((R800 - R670)/(R800 - (6 \times R670) - (7.5 \times R475) + 1))$	Huete et al. (1997)
GI	Greenness index	$R554/R677$	Zarco-Tejada et al. (2005)
GM1	Gitelson and Merzlyak, 94	$R750/R705$	Gitelson and Merzlyak (1994)
GM2	Gitelson and Merzlyak, 94	$R750/R555$	Gitelson and Merzlyak (1994)
GM3	Gitelson and Merzlyak, 97	$R750/R550$	Gitelson and Merzlyak (1997)
GM4	Gitelson and Merzlyak, 97	$R750/R700$	Gitelson and Merzlyak (1997)
GNDVI	Green Normalised Difference VI	$(R780 - R550)/(R780 + R550)$	Gitelson et al. (1996)
GRG	Gitelson ratio green	$(R800/R550) - 1$	Gitelson et al. (2003)
HNDVI2	Hyperspectral normalised difference VI	$(R827 - R668)/(R827 + R668)$	Oppelt and Mauser (2004)
LIC1	Lichtenthaler Index 1	$(R800 - R680)/(R800 + R680)$	Lichtenthaler et al. (1996)
LIC2	Lichtenthaler Index 2	$R440/R690$	Lichtenthaler et al. (1996)
LIC3	Lichtenthaler Index 3	$R440/R740$	Lichtenthaler et al. (1996)
Macc01	Macc 01	$(R780 - R710)/(R780 - R680)$	Maccioni et al. (2001)
MCARI	Modified chlorophyll absorption ratio index	$((R700 - R670) - 0.2 \times (R700 - R550)) \times (R700/R670)$	Daughtry et al. (2000)
MCARI1	Mod. Chlorophyll absorption ratio index 1	$1.2 \times (2.5 \times (R800 - R670) - 1.3 \times (R800 - R550))$ $1.5 \times (2.5 \times (R800 - R670) - 1.3 \times (R800 - R550))$	Haboudane et al. (2004)
MCARI2	Mod. Chlorophyll absorption ratio index 2	$((2 \times R800 + 1)^2 - (6 \times R800 - 5 \times (R670^{0.5}))^{0.5} - 0.5)$	Haboudane et al. (2004)
MCARI3	Revised MCARI	$((R750 - R705) - 0.2 \times (R750 - R550)) \times (R750/R705)$	Wu et al. (2008)
McM_94	McMurtrey, 1994	$R700/R670$	McMurtrey Iii et al. (1994)
mND	Modified normalised difference	$(R750 - R445)/(R750 + R705 - 2 \times R445)$	Sims and Gamon (2002)
mNDVI	Modified NDVI	$(R750 - R705)/(R750 + R705)$	Gitelson and Merzlyak (1994)
mNDVI1	Modified NDVI	$(R755 - R745)/(R755 + R745)$	Mutanga and Skidmore (2004)
mNDVI8	Modified NDVI	$(R755 - R730)/(R755 + R730)$	Mutanga and Skidmore (2004)
mNDVIre	Modified NDVI red edge	$(R750 - R705)/(R750 + R705 - 2 \times R445)$	Sims and Gamon (2002)
mSAVI	Modified Soil Adjusted VI	$0.5 \times (2 \times R800 + 1 - (((2 \times R800 + 1)^2 - 8 \times (R800 - R670))^{0.5}))$	Qi et al. (1994)
mSR	Modified Simple Ratio	$((R800/R670) - 1)/((R800/R670) + 1)^{0.5}$	Chen (1996)

Appendix 1. Summary of Indices used within this study (cntd).

Index	Full name	Equation	Reference
mRESRI	Modified Red Edge Simple Ratio	$(R750 - R445)/(R705 - R445)$	Sims and Gamon (2002)
MTCI	MERIS terrestrial chlorophyll index	$(R754 - R709)/(R709 - R681)$	Dash and Curran (2004)
mTVI1	Modified Triangular VI 1	$1.5 \times (1.2 \times (R712 - R550) - 2.1 \times (R670 - R550))$ $1.5 \times (1.2 \times (R800 - R550) - 2.5 \times (R670 - R550))$	Guan and Liu (2009)
mTVI2	Modified Triangular VI 2	$((2 \times R800 + 1)^2) - ((6 \times R800) - 5 \times (R670^{0.5}))^{0.5} - 0.5$	Haboudane et al. (2004)
NDVI	Normalised difference vegetation index	$(R800 - R670)/(R800 + R670)$	Rouse Jr et al. (1974)
NDVI2	Normalised difference vegetation index 2	$(R800 - R680)/(R800 + R680)$	Rouse Jr et al. (1974)
NDVI3	Normalised difference vegetation index 3	$(R831 - R667)/(R831 + R667)$	Merton (1998)
NDVI4	Normalised difference vegetation index 4	$(R774 - R667)/(R774 + R667)$	Zarco-Tejada et al. (1999)
NPCI	Normalised pigment chlorophyll ratio index	$(R680 - R430)/(R680 + R430)$	Peñuelas et al. (1994)
NPQI	Normalised phaeophytinization index	$(R415 - R435)/(R415 + R435)$	Barnes et al. (1992)
OSAVI	Optimised soil adjusted VI	$1.16 \times (R800 - R670)/(R800 + R670 + 0.16)$	Rondeaux et al. (1996)
rOSAVI	Revised OSAVI	$1.16 \times (R750 - R705)/(R750 + R705 + 0.16)$	Wu et al. (2008)
PRI	Photochemical Reflectance Index	$(R531 - R570)/(R531 + R570)$	Gamon et al. (1992)
PSND_680	Pigment specific normalised difference 680	$(R800 - R680)/(R800 + R680)$	Blackburn (1998)
PSND_635	Pigment specific normalised difference 635	$(R800 - R635)/(R800 + R635)$	Blackburn (1998)
PSSR_A	Pigment specific simple ratio Chl a	$R800/R680$	Blackburn (1998)
PSSR_B	Pigment specific simple ratio Chl b	$R800/R635$	Blackburn (1998)
RDVI	Renormalised difference VI	$(NDVI2 \times DVI)^{0.5}$	Roujean and Breon (1995)
RENDVI	Normalised difference VI – red edge	$(R750 - R705)/(R750 + R705)$	Gitelson and Merzlyak (1994)
RGI	Red Green Ratio Index	$R690/R550$	Zarco-Tejada et al. (2005)
Rre	Reflectance at the inflection point	$(R670 + R780)/2$	Croft et al. (2014)
RR	Reciprocal reflectance	$1/R700$	Gitelson et al. (1999)
SIPI [680]	Structure insensitive pigment index [680]	$(R800 - R445)/(R800 - R680)$	Penuelas et al. (1995a)
SIPI [705]	Structure insensitive pigment index [705]	$(R800 - R445)/(R800 + R705)$	Penuelas et al. (1995a)
SR	Simple ratio	$R774/R677$	Chen (1996)
SR VI	Simple ratio VI	$R800/R670$	Jordan (1969)
SR VIb	Simple ratio VI [750, 550]	$R750/R550$	Gitelson and Merzlyak (1997)
SRPI	Simple ratio pigment index	$R430/R680$	Penuelas et al. (1995a)
TCARI	Transformed chlorophyll absorption ratio index	$3 \times ((R700 - R670) - 0.2 \times (R700 - R550) \times (R700/R670))$	Haboudane et al. (2002)
RTCARI	Revised Transformed chlorophyll absorption index	$3 \times ((R750 - R705) - 0.2 \times (R750 - R550) \times (R750/R705))$	Wu et al. (2008)
TVI	Triangular VI	$0.5 \times (120 \times (R750 - R550) - 200 \times (R670 - R550))$	Broge and Leblanc (2001)
VI	Vegetation Index	$(R700 - R670)/(R700 + R670)$	Gitelson et al. (2002a)
VOG1	Vogelmann index	$R740/R720$	Vogelmann et al. (1993)
VOG2	Vogelmann index	$(R734 - R747)/(R715 + R726)$	Vogelmann et al. (1993)
VOG3	Vogelmann index	$(R734 - R747)/(R715 + R720)$	Vogelmann et al. (1993)
ZM	Zarco and Miller	$R750/R710$	Zarco-Tejada et al. (2001)
MCARI_OSAVI	Ratio of MCARI to OSAVI	$MCARI/OSAVI$	
MCARI3_rOSAVI	Ratio of rMCARI/rOSAVI	$rMCARI/rOSAVI$	Wu et al. (2008)
RTCARI_ROSAVI	Ratio of revised TCARI to revised OSAVI	$RTCARI/ROSAVI$	Wu et al. (2008)
TCARI_OSAVI	Ratio of TCARI to OSAVI	$TCARI/OSAVI$	